Erasmus University Rotterdam

Erasmus School of Economics

Master Thesis Econometrics and Management Science - Quantitative Finance

Global Yield Factors in a Hierarchical Stochastic Volatility Dynamic Nelson-Siegel Approach

Thijs Omloo (509936to)

Supervisor:	M. van der Wel
Second assessor:	A. Quaini
Date final version:	August 16, 2024

Abstract

Understanding the dynamics of the volatility of global bond markets is of great importance, especially in risk management. This paper proposes a Hierarchical Stochastic Volatility dynamic Nelson-Siegel model to capture the global dynamics of volatility across major bond markets, specifically Germany, the US, Japan, and the UK. The model is an extension on the work of Diebold et al. (2008) on global yield factors. Using Bayesian Markov Chain Monte Carlo simulations, I show that the global yield factors exhibit substantial time-varying volatility, which increases during economic crises. The volatility of the global curvature factor closely resembles the MOVE index, a US Treasury volatility proxy. Furthermore, the analysis re-evaluates the connection between the global factors and macroeconomic fundamentals, revealing a weakening link between the global level factor and expected inflation after the Great Financial Crisis. Additionally, the global slope factor is found to be strongly negatively correlated with the G-7 unemployment rate.

Keywords: Global Factors, Dynamic Nelson-Siegel, Stochastic Volatility, Bayesian Econometrics, Time-Varying Parameters

Contents

1 Introduction **3**

2 Modeling Framework **5**

2.1 The Dynamic Nelson-Siegel Model 6

2.2 Multi-Country Framework 6

3 Model Estimation **9**

3.1 State-Space Form 9

3.2 Estimation Procedure 12

3.3 Initializations and Priors 15

4 Data **15**

4.1 Government Bond Yield Data 16

4.2 Macroeconomic Variables 19

5 Empirical Results **20**

5.1 Global Factors 20

5.2 Macroeconomic Links 25

5.3 Country Factors 28

5.4 Variance Decomposition 32

5.5 Goodness of Fit 33

6 Conclusion **37**

A Gibbs Sampler **40**

B Derivation of the Posterior Distributions **41**

B.1 Derivation of the Time-Invariant Parameter Posterior Distributions 41

B.2 Derivation of the Country Factors Posterior Distribution 43

B.3 Derivation of the Carter and Kohn algorithm 44

C Data and Tickers **45**

D Estimation Results **46**

1 Introduction

The term structure of interest rates contains valuable information about the macroeconomy and serves as a crucial tool in areas such as bond pricing, portfolio management, and asset allocation. Due to its capability of capturing a wide variety of shapes and its relatively simple estimation, using latent factors to model the yield curve is a popular approach in literature (e.g. Diebold and Li (2006)). Domestic yield curves have been shown to interact and evolve dynamically, and to be driven by so-called "global" yield factors, which are derived using the aforementioned latent factors of several countries (e.g. Diebold et al. (2008) and Abbritti et al. (2013)). These global factors explain a large portion of national variances, showcasing their importance. Additionally, several papers link these global factors with macroeconomic fundamentals, such as expected inflation, real activity, and economic uncertainty and sentiment measures (e.g. Jotikasthira et al. (2015) and Byrne et al. (2019)). However, much of the literature on global yield modeling overlooks time-varying volatility in these underlying global yield factors. Incorporating time-varying volatility into global bond market models is crucial for risk management policymakers, as it more accurately reflects real-world conditions and accounts for the risks associated with changes in bond market volatility.

This paper aims to extend the literature on global yield factors by incorporating stochastic volatility in these global factors. By analyzing these stochastic processes, I aim to obtain more insights into the dynamics and the driving forces behind volatility of the global bond market. More specifically, I expand the pioneering work of Diebold et al. (2008) on global factors using a Hierarchical Stochastic Volatility dynamic Nelson-Siegel model. This model is based on the work of Tornese (2023), who conducts similar research on the integration of Eurozone bond markets. For the stochastic volatility method, I opt for the framework of Hautsch and Yang (2012), specifically designed for yield curve modeling. My analysis focuses on government bond yields of Germany, the United States, Japan, and the United Kingdom over the past 30 years. I utilize the one-step estimation method of Byrne et al. (2019) in combination with the stochastic volatlity estimation procedure of Hautsch and Yang (2012), which involve Bayesian Markov Chain Monte Carlo (MCMC) simulations that account for parameter uncertainty across all estimated parameters. Using fresh data and a one-step estimation technique, I reassess the global factors' links with macroeconomic fundamentals found in the literature. In addition, the importance of the Bayesian MCMC estimation method is evaluated.

An important cornerstone in term structure modeling is the Nelson-Siegel model

proposed by Nelson and Siegel (1987), which introduces three parameters to explain the yield curve. Diebold and Li (2006) extend this model by allowing the three parameters to vary over time and model them using (V)AR specifications, thereby proposing the Dynamic Nelson-Siegel (DNS) model. In this approach, the three time-varying parameters are treated as latent variables, and are interpreted as the level, slope, and curvature factor of the yield curve. Diebold et al. (2006) employ the same state-space representation, incorporating macroeconomic indicators to enhance the fitting and forecasting of the yield curve. Both DNS models outperform standard time series models in forecasting and are, therefore, widely used in modeling the term structure of interest rates.

Most of the existing literature focuses on modeling the term structure of a single country, thereby ignoring the relationship between cross-country bond yields. Diebold et al. (2008) initiated the literature on multi-country term structure modeling by expanding the DNS model. Using the bond yield data of Germany, the US, Japan, and the UK, their study highlights the existence of a global level and slope factor that explain a large part of national variances. In addition, their global level factor shares a correlation of 0.75 with the G-7 inflation. Jotikasthira et al. (2015) and Byrne et al. (2019) delve deeper into the driving forces behind global bond yields, combining latent factors and macroeconomic fundamentals to explain them. Jotikasthira et al. (2015) find that global inflation and the US level factor explain over 70% of German and UK yields. Similarly, Byrne et al. (2019) demonstrate that economic and sentiment measures account for a large portion of the information in global yield factors. Furthermore, Tornese (2023) extends the work of Diebold et al. (2008) by incorporating stochastic volatility into their model in a study on the driving forces behind Eurozone bond markets.

The majority of empirical studies on term structure modeling assume constant interest rate volatility. However, in the DNS literature, Koopman et al. (2010) introduce the concept of time-varying volatility in interest rates, incorporating it directly into the yield processes through a common component following a univariate GARCH process. Hautsch and Ou (2008) take a different approach, capturing stochastic volatility directly within the underlying yield factors, where the resulting volatility processes follow a first-order autoregressive process. Byrne et al. (2019) allow for stochastic volatility in the global yield factors by using a forgetting factor. However, since the forgetting factor introduces prior bias, Tornese (2023) adopt the stochastic volatility approach of Cogley and Sargent (2005), specialized for VAR models. Under certain assumptions, this approach models the stochastic volatility processes as a random walk. Furthermore, Hautsch and Yang (2012) improve the computational effi-

ciency of the approach of Hautsch and Ou (2008). The resulting framework uses Bayesian Markov Chain Monte Carlo simulations, and opposite to Tornese (2023), does not assume high persistence in the stochastic volatility processes. Therefore, I use their method.

The one-step Bayesian MCMC estimation method extracts country-specific factors, global factors, and the stochastic volatility processes within the global factors. The empirical results show strong evidence supporting the time-varying volatility within the global yield factors. The stochastic volatility processes are highly persistent, show signs of co-movement and increase in periods of economic downturns. Additionally, the volatility of the global curvature factor closely resembles the MOVE index, a US Treasury volatility proxy. Furthermore, the flexible framework highlights the influence of common forces on the national variances, which peaks during times of high volatility. However, the impact of global factors on their country-specific counterpart has decreased compared to Diebold et al. (2008), indicating a stronger presence of idiosyncratic forces in domestic bond markets post-2008.

Examining the global factors' connection to real world conditions reveals that the relationship between the expected inflation and the global factor has weakened since the Great Recession. The global slope factor, however, is highly negatively correlated with the G-7 unemployment rate. The results show no significant evidence that supports the co-movement between the global factors and economic uncertainty and sentiment measures. Furthermore, the incorporation of parameter uncertainty in the country-specific factors yields minimal differences compared to the OLS estimation in Diebold et al. (2008) for the country level and slope factors. For the country curvature factors, however, a greater degree of divergence between the results of the two estimation methods is found.

The remainder of this paper is as follows. Section 2 introduces the Hierarchical Stochastic Volatility dynamic Nelson-Siegel model. Section 3 illustrates the Bayesian Markov Chain Monte Carlo procedure used for estimation. In section 4, the data used in the empirical study is described. Section 5 presents the empirical results, while section 6 summarizes and concludes the research.

2 Modeling Framework

In this chapter, I first introduce the Dynamic Nelson-Siegel (DNS) model proposed by Diebold and Li (2006) in section 2.1. Then, in section 2.2, I present the Hierarchical Stochastic Volatility dynamic Nelson-Siegel (HSV-DNS) model, which builds on the DNS model.

2.1 The Dynamic Nelson-Siegel Model

Nelson and Siegel (1987) introduce a parsimonious way to model the yield curve by several latent factors. Diebold and Li (2006) extend this approach and introduce the DNS model, which comes down to the following. For a yield series $y_t(\tau_j)$ at time t with the set of maturities $\{\tau_j\}_{j=1}^m$ the yield curve is described by the following formulation

$$y_t(\tau_j) = l_t + s_t\left(\frac{1-e^{-\lambda\tau_j}}{\lambda\tau_j}\right) + c_t\left(\frac{1-e^{-\lambda\tau_j}}{\lambda\tau_j} - e^{-\lambda\tau_j}\right) + v_t(\tau_j), \tag{1}$$

where λ is a fixed coefficient that determines the exponential decay of the second and third factor, and $v_t(\tau_j)$ represents the Gaussian distributed pricing error. The formula shows that the latent factors l_t, s_t, and c_t, and their respective factors loadings, determine the yield curve. The first factor loading takes the value 1, indicating that the loading influences the overall level of yields of all maturities. Therefore, l_t is interpreted as the level factor. The second factor loading converges to one as $\tau \to 0$ and to zero as $\tau \to \infty$. This suggests that it primarily affects short-term rates, thus shaping the yield curve's slope. Consequently, s_t is interpreted as the slope factor. The third factor loading converges to zero for both $\tau \to 0$ and $\tau \to \infty$, and is concave in the maturity τ. Therefore, it mostly influences medium-term rates, hence shaping the curvature of the yield curve. Thus, c_t is interpreted as the curvature factor. The DNS model and its interpretation of the latent factors are exploited in the multi-country framework, presented in the next section.

2.2 Multi-Country Framework

Diebold et al. (2008) pioneered multi-country term structure modeling by extending the DNS model such that for each country $i = 1, ..., N$ at time t for maturities $\{\tau_j\}_{j=1}^m$, the dynamics of the yield curve are modeled by

$$y_{i,t}(\tau_j) = l_{i,t} + s_{i,t}\left(\frac{1-e^{\lambda\tau_j}}{\lambda\tau_j}\right) + c_{i,t}\left(\frac{1-e^{\lambda\tau_j}}{\lambda\tau_j} - e^{-\lambda\tau_j}\right) + v_{i,t}(\tau_j), \tag{2}$$

where $y_{i,t}(\tau_j)$ is the zero-coupon bond yield at time t of a treasury bond of country i with maturity τ_j. The latent variables $l_{i,t}, s_{i,t}, c_{i,t}$ are the level, slope, and curvature factor for each country i, respectively, as explained in the previous section. The decay factor λ is set constant across countries and time. Furthermore, $v_{i,t}(\tau_j)$ are the pricing errors. I assume the vector of pricing errors $v_{i,t} = \{v_{i,t}(\tau_1), ..., v_{i,t}(\tau_m)\}'$ to follow the normal distribution

$\mathcal{N}(0, \Sigma_{v_i})$, where Σ_{v_i} is a m x m diagonal matrix. The assumption of uncorrelated pricing errors across maturities is common in literature and arises because the zero-coupon yields used in estimation are bootstrapped from coupon-bearing bonds, leading to measurement errors across maturities which are not correlated. For parsimony, Diebold et al. (2008) omit the curvature factor from their model. However, Mönch (2012) and Abbritti et al. (2013) suggest that incorporating the curvature factor is beneficial for uncovering the dynamics of the term premium, and therefore I include it.

Diebold and Li (2006) recognize the strong persistence in the latent factors, implying these factors can be forecasted with high precision. Therefore, the DNS model allows the latent factors to follow a first-order autoregressive process. The multi-country yield curve framework deviates from this approach by allowing the country-specific latent factors to load on common factors, such that

$$f_{i,t} = \alpha^f_{i,t} + \beta^f_i F_t + e^f_{i,t}, \tag{3}$$

where $f_{i,t} \in [l_{i,t}, s_{i,t}, c_{i,t}]$ denotes the country factors, $\beta^f_i \in [\beta^l_i, \beta^s_i, \beta^c_i]$ are the loadings on the global factor, and $F_t \in [L_t, S_t, C_t]$ are the global factors, specifically the global level, slope and curvature factor. Diebold et al. (2008) and Byrne et al. (2019) endow autoregressive properties on the disturbances $e^f_{i,t} \in [e^l_{i,t}, e^s_{i,t}, e^c_{i,t}]$, and fix each $\alpha^f_{i,t} \in [\alpha^l_{i,t}, \alpha^s_{i,t}, \alpha^c_{i,t}]$ over time. However, the introduction of the country-specific time-varying intercept $\alpha^f_{i,t}$ by Tornese (2023) allows the innovations $e^f_{i,t}$ to be uncorrelated across i and t, and to follow the normal distribution $\mathcal{N}(0, \sigma^2_{e^f_i})$. Furthermore, the global factors and their loadings are separately identified by assuming $\sum_{i=1}^{N} \beta^f_i = 1$. This assumption allows for the comparison of the relative influence of the common forces on each country.

To complete the hierarchical features of the model, the law of motion of the time-varying intercepts $\alpha^f_{i,t}$ and the global factors $\bar{F}_t = \{L_t, S_t, C_t\}'$ is given by

$$\alpha^f_{i,t} = \gamma^f_i + \psi^f_i \, \alpha^f_{i,t-1} + u^f_{i,t} \tag{4}$$

$$\bar{F}_t = C + \Phi \bar{F}_{t-1} + \eta_t, \tag{5}$$

where $\gamma^f_i \in [\gamma^l_i, \gamma^s_i, \gamma^c_i]$ and $\psi^f_i \in [\psi^l_i, \psi^s_i, \psi^c_i]$ are the coefficients of the first-order autoregressive process that describes the dynamics of the time-varying intercept $\alpha^f_{i,t}$ of the country factors for each country i. The intercept term γ^f_i is identified as $\gamma^f_i = \mu_{\alpha^f_i}(1 - \psi^f_i)$, where $\mu_{\alpha^f_i}$ denotes the mean of the serie $\alpha^f_{i,t}$. In the model, the error terms $u^f_{i,t}$ follow the normal distribution $\mathcal{N}(0, \sigma^2_{u^f_i})$. Furthermore, the intercept vector $C = \{c^L, c^S, c^C\}'$ of the vector

autoregressive process of the global factors is identified as $C = (\mathrm{I} - \Phi)\mu_F$, where the vector $\mu_F = \{\mu_L, \mu_S, \mu_C\}'$ contains the means of the global factors. Diebold et al. (2008) and Tornese (2023) validate the use of a diagonal coefficient matrix Φ, therefore I set $\Phi = diag\{\phi^L, \phi^S, \phi^C\}$. Furthermore, assume the error terms $\eta_t = \{\eta_t^L, \eta_t^S, \eta_t^C\}'$ to be normally distributed as $\eta_t \sim \mathcal{N}(0, \Omega_t)$. The variance term Ω_t introduces stochastic volatility into the model.

The proposed model deviates from Tornese (2023) in three ways. Tornese (2023) allows the factor loadings β_i^f to have random walk properties, the variance of error terms $u_{i,t}^f$ to incorporate time variation, and the global factor error terms η_t to follow the stochastic volatility approach of Cogley and Sargent (2005). The focus of this paper lies not in the changing dynamics of the countries over time and therefore, to avoid overfitting and increase computational efficiency, I assume β_i^f and the variance of $u_{i,t}^f$ to be constant over time. However, since this paper focusses on incorporating stochastic volatility in the variance of the global factor error terms, I adopt the more advanced stochastic volatility approach of Hautsch and Yang (2012), designed specifically for DNS models.

The stochastic volatility approach by Hautsch and Yang (2012) performs a Cholesky decomposition to obtain $\Omega_t = \Sigma_{\eta,t}\Sigma_{\eta,t}^T$, specified as

$$diag(\ln \Sigma_{\eta,t}\Sigma_{\eta,t}') = \begin{pmatrix} h_t^L \\ h_t^S \\ h_t^C \end{pmatrix} \tag{6}$$

$$\begin{pmatrix} h_{t+1}^L - \mu_h^L \\ h_{t+1}^S - \mu_h^S \\ h_{t+1}^C - \mu_h^C \end{pmatrix} = \begin{pmatrix} \pi^L & 0 & 0 \\ 0 & \pi^S & 0 \\ 0 & 0 & \pi^C \end{pmatrix} \begin{pmatrix} h_t^L - \mu_h^L \\ h_t^S - \mu_h^S \\ h_t^C - \mu_h^C \end{pmatrix} + \begin{pmatrix} \sigma^L \xi_t^L \\ \sigma^S \xi_t^S \\ \sigma^C \xi_t^C \end{pmatrix}, \tag{7}$$

where $\xi_t^F \overset{i.i.d.}{\sim} \mathcal{N}(0,1)$, and π^F is the first-order autoregressive coefficient of the global factors for $F = L, S, C$. Tornese (2023) assumes all π^F coefficients to be equal to one. The disturbances η_t are assumed to be contemporaneously uncorrelated, resulting in a diagonal covariance matrix Ω_t at each time t. Then, transforming the model back to η_t yields

$$\begin{pmatrix} \eta_t^L \\ \eta_t^S \\ \eta_t^C \end{pmatrix} = \begin{pmatrix} e^{h_t^L/2} & 0 & 0 \\ 0 & e^{h_t^S/2} & 0 \\ 0 & 0 & e^{h_t^C/2} \end{pmatrix} \begin{pmatrix} \zeta_t^L \\ \zeta_t^S \\ \zeta_t^C \end{pmatrix}, \tag{8}$$

where $\zeta_t^F \overset{i.i.d.}{\sim} \mathcal{N}(0,1)$ for $F = L, S, C$. Thus, h_t^F with $F = L, S, C$ are the latent stochastic volatility processes of the global factors and can be summarized in the vector $h_t =$

$\{h_t^L, h_t^S, h_t^C\}'$. Due to the transformation, the components h_t^L, h_t^S, and h_t^C can be interpreted as the time-varying volatilities of the extracted global level, slope, and curvature factor. Since the factor h_t^L captures the uncertainty related to the volatility of the global level factor, thereby influencing the bond yields of different maturities equally, it can be seen as a model implied proxy of the global bond market volatility. Furthermore, h_t^L can be interpreted as the yield curve slope volatility since it captures the time-variation associated with the yield spreads. Lastly, the stochastic volatility component h_t^C captures the volatility related to portfolios that are dominated by mid-term maturities and can therefore be interpreted as yield curve curvature volatility.

3 Model Estimation

In this chapter, I propose the models and methods used for factor extraction and parameter estimation. Section 3.1 presents the state-space systems used to exploit the Bayesian Markov Chain Monte Carlo (MCMC) simulations estimation method, which is described in section 3.2. Section 3.3 discusses the initialization techniques and the choice of priors for the MCMC simulations.

3.1 State-Space Form

Section 2.2 introduces the HSV-DNS model. The hierarchical nature of the model introduces four sets of latent variables: the country factors f_t, the global factors $\bar{F}_t$, the time-varying intercepts α_t, and the volatility processes h_t. These latent time series are extracted by exploiting state-space systems, which I present in this section.

To identify the country factors f_t, I follow Tornese (2023), who shows that one can extract the country factors f_t out of the government bond yields using the following state space representation

$$y_t = \Pi(\lambda) f_t + v_t, \qquad v_t \sim \mathrm{N}(0, \Sigma_v), \tag{9}$$

$$f_t = \alpha_t + \mathrm{B}\bar{F}_t + e_t, \qquad e_t \sim \mathrm{N}(0, \Sigma_e), \tag{10}$$

for $t = 1, ..., T$ where $y_t = \{y_{1,t}(\tau_1), y_{1,t}(\tau_2), ..., y_{N,t}(\tau_m)\}'$, $f_t = \{l_{1,t}, s_{1,t}, ..., c_{N,t}\}'$, $\alpha_t = \{\alpha^l_{1,t}, \alpha^s_{1,t}, ..., \alpha^c_{N,t}\}'$, $e_t = \{e^l_{1,t}, e^s_{1,t}, ..., e^c_{N,t}\}'$, $v_t = \{v_{1,t}(\tau_1), v_{1,t}(\tau_2), ..., v_{N,t}(\tau_m)\}'$, and

$$\Pi(\lambda) = \begin{bmatrix} 1 & \left(\frac{1-e^{-\lambda\tau_1}}{\lambda\tau_1}\right) & \left(\frac{1-e^{-\lambda\tau_1}}{\lambda\tau_1} - e^{-\lambda\tau_1}\right) & 0 & \dots & \dots & 0 \\ 1 & \left(\frac{1-e^{-\lambda\tau_2}}{\lambda\tau_2}\right) & \left(\frac{1-e^{-\lambda\tau_2}}{\lambda\tau_2} - e^{-\lambda\tau_2}\right) & 0 & \dots & \dots & 0 \\ \vdots & \vdots & \vdots & \ddots & \vdots & \vdots & \vdots \\ 0 & \dots & \dots & \dots & 1 & \left(\frac{1-e^{-\lambda\tau_m}}{\lambda\tau_m}\right) & \left(\frac{1-e^{-\lambda\tau_m}}{\lambda\tau_m} - e^{-\lambda\tau_m}\right) \end{bmatrix},$$

$$\mathrm{B} = \begin{bmatrix} \beta^l_1 & 0 & 0 \\ 0 & \beta^s_1 & 0 \\ \vdots & \vdots & \vdots \\ 0 & 0 & \beta^c_N \end{bmatrix}.$$

Tornese (2023) highlights a key distinction in transition eq.(10) from Diebold et al. (2008), Moench et al. (2013), and Byrne et al. (2019): the assumption of serially uncorrelated error terms $e^f_{i,t}$, achieved through the time-varying intercept $\alpha^f_{i,t}$. This approach eliminates the need for the quasi-differencing operator, making the country factors f_t exclusively dependent on exogenous variables and therefore omitting the need to perform the Carter and Kohn (1994) backwards smoothing algorithm. As a result, the country factors f_t can be sampled from the normal distribution where the mean and variance are obtained through a simplified Kalman Filter, in which only the noise e_t has to be separated from f_t.

Next, I present the state-space system used to extract the global factors F_t. The coefficient matrix Φ and variance matrix Ω_t are diagonal. Therefore, the time series of the global factors L_t, S_t, and C_t can be extracted separately. For illustration purposes, I present the state-space form needed to extract the global level factor L_t as

$$\begin{bmatrix} l_{1,t} \\ \vdots \\ l_{N,t} \end{bmatrix} = \begin{bmatrix} \alpha^l_{1,t} \\ \vdots \\ \alpha^l_{N,t} \end{bmatrix} + \begin{bmatrix} \beta^l_{1,t} \\ \vdots \\ \beta^l_{N,t} \end{bmatrix} L_t + \begin{bmatrix} e^l_{1,t} \\ \vdots \\ e^l_{N,t} \end{bmatrix}, \qquad \begin{bmatrix} e^l_{1,t} \\ \vdots \\ e^l_{N,t} \end{bmatrix} \sim \mathrm{N}(0, \Sigma_{e^l}) \tag{11}$$

$$L_t = \phi^L L_{t-1} + \eta^L_t, \qquad \Omega^L_t \sim \mathrm{N}(0, \omega^L_t), \tag{12}$$

where ϕ^L and ω^L_t represent the diagonal elements of Φ and Ω_t respectively, corresponding with the global level factor. This representation allows for the use of the Carter and Kohn (1994) (CK) backwards smoothing algorithm. The CK algorithm performs the Kalman Filter, after

which the estimated states and variances are smoothed using a backward recursion method, the Kalman Smoother. The smoothed estimates are then used to sample the unobserved states.

For extracting the time-varying intercepts $\alpha^f_{i,t}$, I again employ the CK backwards smoothing algorithm. The assumption of serial uncorrelated error terms $u^f_{i,t}$ across i and t, allows for extracting each $\alpha^f_{i,t}$ separately. For example, for the level factor of country $i = 1$, the time-varying intercept $\alpha^l_{1,t}$ can be extracted using the following state space representation

$$l_{1,t} = \alpha^l_{1,t} + \beta^l_1 L_t + e^l_{1,t}, \qquad e^l_{1,t} \sim \mathcal{N}(0, \sigma^2_{e^l_1}), \tag{13}$$

$$\alpha^l_{1,t} = \gamma^l_1 + \psi^l_1 \, \alpha^l_{1,t-1} + u^l_{1,t}, \qquad u^l_{1,t} \sim \mathcal{N}(0, \sigma^2_{u^l_1}). \tag{14}$$

Finally, define $\Gamma = (\gamma^l_1, \gamma^s_1, ...\gamma^c_N)$ and $\Psi = (\psi^l_1, \psi^s_1, ..., \psi^c_N)$. This notation will be useful for the next subsection.

Lastly, I propose the state-space representation Hautsch and Yang (2012) use to extract the volatility processes h_t. Define

$$\begin{aligned}
e^{h_t/2} &= diag\{e^{h^L_t/2}, e^{h^S_t/2}, e^{h^C_t/2}\}, \\
\mu_h &= \{\mu_{h^L}, \mu_{h^S}, \mu_{h^C}\}', \\
\pi &= diag\{\pi^L, \pi^S, \pi^C\}' \\
\Sigma_h &= diag\{\sigma^2_{h^L}, \sigma^2_{h^S}, \sigma^2_{h^C}\}', \\
\xi_t &= \{\xi^L_t, \xi^S_t, \xi^C_t\}', \\
\zeta_t &= \{\zeta^L_t, \zeta^S_t, \zeta^C_t\}',
\end{aligned}$$

such that eq.(7) and eq.(8) can be rewritten as

$$\eta_t = e^{h_t/2}\zeta_t, \tag{15}$$

$$h_{t+1} - \mu_h = \pi(h_t - \mu_h) + \Sigma^{1/2}_h \xi_t. \tag{16}$$

This transformation yields a state-space system where eq.(15) serves as the measurement equation and eq.(16) as the transition equation. However, the measurement equation is non-linear and non-Gaussian, which are crucial assumptions for the CK algorithm. Nonetheless, S. Kim et al. (1998) show that this equation can be transformed into a mixture of normals model, thereby enabling the use of the Kalman Filter and a simulation smoother. Their

approach uses the transformation

$$\ln \eta_t^2 = h_t + \ln \zeta_t^2, \tag{17}$$

to introduce linearity and, under the right specifications, normality. Define $y_t^* = \ln(\eta_t^2 + c)$ and $z_t = \ln \zeta_t^2$, where c is the "offset" introduced in stochastic volatility literature by Fuller (1996), and typically set to $c = 0.001$. Substituting these transformations yields the following state-space system

$$y_t^* = h_t + z_t \tag{18}$$

$$h_{t+1} - \mu_h = \pi(h_t - \mu_h) + \sigma\xi_t. \tag{19}$$

The stochastic volatility processes h_t can now be extracted using the S. Kim et al. (1998) mixture of normals approach, which I explain in depth in the next section.

3.2 Estimation Procedure

Diebold et al. (2008) pioneered the estimation of multi-country DNS models and use a two-step estimation approach. In the first step, they perform OLS estimation in eq.(2) to obtain the country-specific factors. These factors are used as observed variables in the second step, where they perform Bayesian MCMC simulations to obtain the remaining parameters and factors. This approach ignores the parameter uncertainty related to the country-specific factors. Byrne et al. (2019) propose a one-step approach that incorporates the parameter uncertainty of all estimated parameters, by also using MCMC simulations. More specifically, they use the Gibbs Sampler, a statistical method designed to generate a sequence of samples from the joint distribution of a set of variables. This technique is particularly helpful in models with a high number of variables, as it sidesteps the challenge of deriving a closed-form solution for the joint distribution. It does so by iteratively sampling from the conditional distribution of each variable, given the others, until the sequence of samples converges to the joint distribution. In this paper, I follow this approach and specify it specifically for the proposed HSV-DNS model.

To illustrate the process of the Gibbs sampler, I explain a simplified example using Casella and George (1992). In Bayesian analysis, one can sample the parameter of interest θ from its posterior distribution $p(y|\theta)$. To determine this distribution, a prior belief is specified,

and the likelihood function of the data y is utilized. By applying Bayes' rule, we obtain:

$$p(\theta|y) \propto p(\theta)p(y|\theta),$$

where $p(\theta)$ is the prior distribution of parameter θ and $p(y|\theta)$ is the likelihood function of the data y as a function of the model parameters θ.

For Gibbs sampling, let θ be a random vector which can be divided in k blocks with posterior density $p(\theta_1, ..., \theta_k|y)$. Then,

1 : Initialize $\theta^{(0)} = (\theta_1^{(0)}, ..., \theta_k^{(0)})$ and set $m = 0$.

2 : Sample

$$\begin{aligned}
&\theta_1^{(m+1)} \text{ from } p(\theta_1 \mid \theta_1^{(m)}, \theta_2^{(m)}, ..., \theta_k^{(m)}, y) \\
&\theta_2^{(m+1)} \text{ from } p(\theta_2 \mid \theta_1^{(m+1)}, \theta_3^{(m)}, ..., \theta_k^{(m)}, y) \\
&\theta_3^{(m+1)} \text{ from } p(\theta_3 \mid \theta_1^{(m+1)}, \theta_2^{(m+1)}, ..., \theta_k^{(m)}, y) \\
&\qquad\qquad \vdots \\
&\theta_k^{(m+1)} \text{ from } p(\theta_1 \mid \theta_1^{(m+1)}, \theta_2^{(m+1)}, ..., \theta_{k-1}^{(m+1)}, y)
\end{aligned}$$

3 : set $m = m + 1$, and go to step 2.

After the Markov chain has converged, at $m = m^*$, the simulated values $\{\theta^{(m)}, m \geq m^*\}$ can be used as a sample from the joint posterior distribution $p(\theta_1, ..., \theta_k|y)$.

Now let's specify the Gibbs sampler tailored to our model. Let $\Theta = \{\theta, f_t, \bar{F}_t, \alpha_t, H\}$ be the set of variables of interest. Define $\theta = \{\Sigma_v, \Sigma_e, \Sigma_u, \mathrm{B}, C, \Phi, \Gamma, \Psi\}$ as the time-invariant variables unrelated to the stochastic volatility processes h_t and store the variables related to stochastic volatility in $H = \{h_t, s_t, \pi, \mu_h, \Sigma_h\}$. The full procedure of the Gibbs Sampler is shown in Appendix A. For conciseness, I present the summarized version of the Gibbs sampler as follows

1. Initialize Θ
2. Sample the variables in Θ from $\Theta|y_t$ using S replications, where the initial S_0 samples are discarded
   (a) Sample the variables θ from $p(\theta|y_t, f_t, \bar{F}_t, \alpha_t, H)$ using inverse-Gamma and Gaussian distributions
   (b) Sample the country factors f_t from $p(f_{i,t}|y_t, \theta, \bar{F}_t, \alpha_t, H)$ using a simplified Kalman Filter method

(c) Sample the global factors $\bar{F}_t$ from $p(F_t|y_t, \theta, f_t, \alpha_t, H)$ using the Carter and Kohn (1994) algorithm

(d) Sample the idiosyncratic components α_t from $p(\alpha^f_{i,t}|y_t, \theta, f_t, \bar{F}_t, H)$ using the Carter and Kohn (1994) algorithm

(e) Sample the block H from $p(H|y_t, \theta, f_t, \bar{F}_t, \alpha_t)$ using the Hautsch and Yang (2012) approach

The derivations of the posterior density functions of the time-invariant parameters are exhibited in Appendix B.1. Appendix B.2 explains the simplified Kalman Filter used to extract the country factors f_t, while Appendix B.3 gives a detailed derivation of the Carter and Kohn (1994) algorithm. To sample the stochastic volatility processes h_t, S. Kim et al. (1998) show that we can make eq.(18) linear by approximating the distribution of z^F_t as a mixture of Gaussian densities, such that

$$z^F_t|s_t \sim f_{\mathcal{N}}(m_{s_t}, \nu^2_{s_t}), \tag{20}$$

where $f_{\mathcal{N}}(m_{s_t}, \nu^2_{s_t})$ is a Gaussian probability density function, and $s_t \in \{1, 2, ..., 7\}$ denotes the state at time t

$$\mathrm{P}\left[s_t = i\right] = q_i, \qquad i \leq 7, \qquad t \leq T. \tag{21}$$

Table 1: Parameters of the Seven States Gaussian Mixture Distrubition Approximation of z_t

s_t	q_i	m_{s_t}	$\nu^2_{s_t}$
1	0.00730	-11.40039	5.79596
2	0.10556	-5.24321	2.61369
3	0.00002	-9.83726	5.17950
4	0.04395	1.50746	0.16735
5	0.34001	-0.65098	0.64009
6	0.24566	0.52478	0.34023
7	0.25750	-2.35859	1.26261

Table 1 shows the values of the parameters $\{q_i, m_{s_t}, \nu^2_{s_t}\}$ given by S. Kim et al. (1998). By approximating the distribution of z^F_t as a mixture of Gaussian densities, the distribution of $y^*_t \mid s_t, \mu_h, \sigma_h, \pi$ becomes Gaussian and therefore the CK algorithm can be used to sample the stochastic volatility component h_t from $h_t \mid y^*_t, s, \mu_h, \sigma_h, \pi$. Finally, the states s_t can then be sampled from $s_t \mid y^*_t, h_t$, by independently sampling each s_t from its probability mass function

$$\mathrm{P}\left[s_t = i \mid y^*_t, h_t\right] \propto q_i f_{\mathcal{N}}(y^* \mid h_t + \ m_i, \nu^2_i). \tag{22}$$

3.3 Initializations and Priors

Step 1 of the Gibbs sampler is crucial for the estimation process. Poor initialization leads to slow convergence and suboptimal results, and vice versa. The same holds for the choice of priors. In this section, the initialization process and the choice of priors for all parameters in Θ is explained. The country factors $f_{i,t}$ are initialized by performing Ordinary Least Squares (OLS) estimation separately on each country for $t = 1, ..., T$. The global factors F_t are initialized separately using the first principal component obtained from a Principal Component Analysis (PCA) on all related country factors. To initialize the global factors loadings β_i^f, each initialized country factors $f_{i,t}^{OLS}$ regresses on its complementary global factor F_t^{PCA}. The residuals from these regressions are used as the initial values for the time-varying intercepts $\alpha_{i,t}^f$. To initialize all variables in H, I run step 2d of the Gibbs sampler. The remaining variables in θ are initialized by running the step in the Gibbs sampler associated with sampling that specific variable. Furthermore, I specify the values that initialize the CK algorithms. Following Primiceri (2005), the mean and variance of F_0 that start the algorithm are chosen as the full sample mean and four times the variance from the previous iteration. The same approach is used for time-varying idiosyncratic components α_0, and the stochastic volatility processes h_0.

The choice of priors for the (truncated) normal distributions is a bit more tricky. Tornese (2023) calibrates the priors with a small sub-sample of the data, resulting in the loss of these observations. On the contrary, Hautsch and Yang (2012) use diffuse priors in their analysis. I choose to follow this approach, as the small sub-sample may not be representative of the entire sample, and retaining all observations is essential for a robust analysis. Furthermore, the choice of inverse-Gamma priors yields the same trade-off. Hautsch and Yang (2012) use non-informative priors, while Tornese (2023) uses a small subsample to calibrate the priors. Again, I follow Hautsch and Yang (2012). In a robustness check, I used the first 36 (3 years) observations to calibrate the priors and found no sensible changes in the results.

4 Data

This section describes the data used in our empirical study. Section 4.1 shows the government bond yields, and explains them through their summary statistics. In section 4.2, I present the macroeconomic variables that potentially link the driving forces behind the yield data to

real-world conditions.

4.1 Government Bond Yield Data

For the empirical analysis in this thesis, I use monthly data consisting of the constant maturity yields of government zero-coupon bonds from the United States, Germany, Japan, and the United Kingdom, all expressed in local currency terms. The yields are calculated and provided by *Refinitiv Eikon*, which uses the cubic spline method, developed by Waggoner (1997), to extract zero-coupon yields from a variety of liquid instruments. The dataset consists of end-of-month yields for the period of January 1995 till March 2024 for the maturities 3 and 6 months, and 1, 2, 3, 5, 7, and 10 years, with the tickers given in Appendix C.

Figure 1 plots the cross-section of yields over the sample period across countries. Co-movement between the country yields is clearly visible, especially within the level, where we observe a downward trend up to 2020. The variety in yield curve slopes and curvatures is also displayed, highlighted by a concave yield curve at the start and an inverted yield curve at the end of the sample for the US, Germany, and the UK. Furthermore, the figure exhibits distinctions in the magnitude of the level, slope, and curvature movements over time, which could indicate the presence of time-varying volatility in their common driving factors. Interestingly, the behavior of the Japanese yield curve differs from that of the other countries. This divergence can be explained by the Bank of Japan's battle against deflation since the 1990s, resulting in prolonged periods of low and negative interest rates, as shown in the figure.

Table 2 presents the mean, standard deviation, minimum, and maximum as well as the 1-month, 1-year, and 2-year auto-correlations of the yields of a set of maturities for each country. The maturities are chosen based on representability for short-, mid- and long-term government bonds, where the 3-month represents the short-term, 1- and 5-year the mid-term maturities, and the 10-year maturity portrays the long-end of the yield curve. Furthermore, a slope and a curvature proxy are exhibited in the table. The proxy for the slope of the yield curve is defined as $y_t(120) - y_t(3)$, where $y_t(\tau)$ is the yield of a government bond with time-to-maturity τ, measured in months. The curvature proxy is given by the butterfly spread $[y_t(24) - y_t(3)] - [y_t(120) - y_t(24)]$.

Figure 1: Yield Curves across Time ranging from January 1995 till March 2024

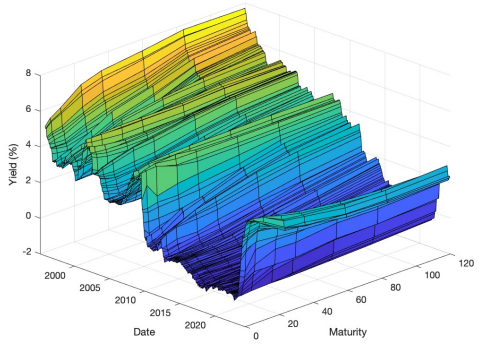

(a) Germany Yield Curve

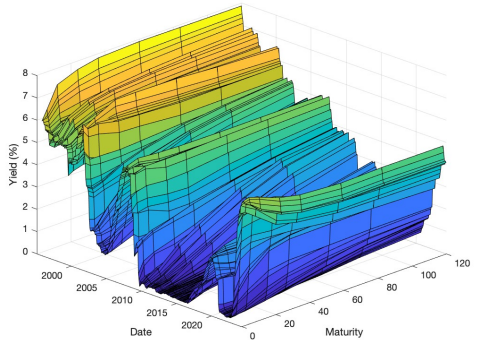

(b) United States Yield Curve

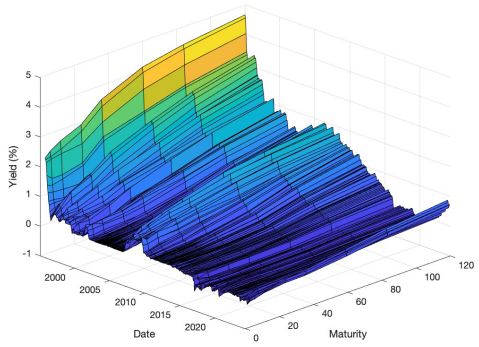

(c) Japan Yield Curve

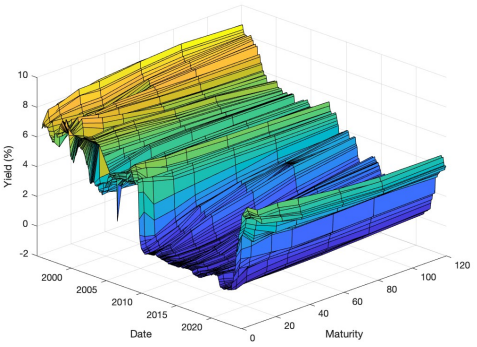

(d) United Kingdom Yield Curve

Note: These figures plot the government bond yields of Germany, the United States, Japan, and the United Kingdom across time and maturity. The sample ranges from January 1995 till March 2024 and considers eight maturities.

Some stylized facts of the yield curve are clearly visible when reviewing the table. The average yield, depicted by the mean, increases as maturities extend. Additionally, yields exhibit high persistence, generally more so for long maturities compared to shorter ones, with the exception of the 10-year UK Gilt. The variances of yields show some interesting properties. For German and Japanese yields, variance increases with maturity. Typically, the long end of the curve is more volatile than the short end. The short end of the curve is closely related to central bank interest rates and their expectations, while the long end is more sensible to changes in macroeconomic conditions. The Bank of Japan's rate has remained between -0.1% and 0.5% throughout the entire sample period. Consequently, the short-end of the Japanese curve has been very stable, and Japan's overall yield curve volatility is considerably lower than in other countries, where central bank rates have been more volatile. For Germany, the summary statistics over the last 30 years indicate that changes in economic factors have had a greater impact on yields than the fluctuations in short-term rates set by the European Central Bank. Furthermore, the positive mean for each slope

proxy, combined with the negative mean for all curvature proxies, confirms the increasingly flattening behaviour of the average yield curves. In addition, the slope of the yield curve is generally less persistent than its curvature, except in Japan. This difference may be due to Japan's long-term economic conditions and monetary policies, which have resulted in stable short-term rates that increased the slope's persistence.

Table 2: Summary Statistics for Government Bond Yields

Country	Maturity	Mean	Std	Min	Max	$\hat{\rho}_1$	$\hat{\rho}_{12}$	$\hat{\rho}_{24}$
United States	3	2.315	2.164	0.005	6.386	0.988	0.745	0.382
	12	2.536	2.177	0.051	7.260	0.987	0.807	0.423
	60	3.231	1.855	0.229	7.890	0.979	0.811	0.582
	120	3.732	1.628	0.562	7.859	0.977	0.819	0.639
	Slope	1.418	1.209	-1.735	3.787	0.964	0.461	0.080
	Curvature	-0.501	0.448	-1.473	0.360	0.978	0.694	0.339
Germany	3	1.631	1.880	-1.020	5.122	0.989	0.807	0.616
	12	1.742	1.908	-0.878	5.780	0.987	0.807	0.622
	60	2.294	2.066	-0.893	7.350	0.985	0.868	0.751
	120	2.876	2.103	-0.728	7.691	0.988	0.882	0.755
	Slope	1.245	0.946	-1.616	3.307	0.956	0.402	0.155
	Curvature	-0.582	0.343	-1.362	0.183	0.957	0.542	0.145
Japan	3	0.113	0.320	-0.470	2.230	0.910	0.428	0.271
	12	0.162	0.364	-0.349	2.620	0.910	0.548	0.339
	60	0.570	0.676	-0.362	4.127	0.941	0.711	0.502
	120	1.110	0.896	-0.280	4.661	0.965	0.786	0.606
	Slope	0.997	0.676	-0.101	2.940	0.972	0.781	0.590
	Curvature	-0.540	0.297	-1.438	-0.082	0.973	0.746	0.567
United Kingdom	3	3.006	2.545	-0.049	7.650	0.991	0.826	0.673
	12	2.978	2.517	-0.071	7.750	0.988	0.841	0.691
	60	3.371	2.300	-0.104	8.651	0.986	0.849	0.703
	120	3.698	2.076	0.140	8.684	0.985	0.839	0.667
	Slope	0.692	1,198	-2.187	3.562	0.957	0.529	0.195
	Curvature	-0.327	0.476	-1.530	0.674	0.974	0.774	0.552

Note: This table exhibits the mean, standard deviation, minimum, maximum, and 1-month, 1-year, and 2-year autocorrelation of the government bond yields of the US, Germany, Japan and the United Kingdom over the period January 1995 to March 2024 for four maturities, corresponding with the short-, mid- and long-end of the yield curve. In addition, the table displays the statistics of a proxy for the slope and curvature factor, defined by $y_t(120) - y_t(3)$ and $[y_t(60) - y_t(3)] - [y_t(120) - y_t(60)]$, respectively.

As a rough proxy for the volatility of stock markets, the literature often opts for absolute returns (see e.g. Ding et al. (1993) and Taylor (2008)). Since bond yields and bond prices are inversely related, I consider the one-month absolute yield change as a rough proxy for the underlying volatility of the domestic bond markets. Table 3 presents the correlation coefficients between the absolute yield changes of the considered countries for the 3 month, 3 year, and 10 year maturities. Here, the 3 month maturity represents the short-term of the yield curve, 3 year the mid-term, and the 10 year maturity is considered the long-term of the curve. When analyzing the table, two observations stand out: first, the absolute yield changes in Japan show weak co-movement with those of other countries. Second, for Germany, the US, and the UK, there is noticeable commonality in absolute yield changes, which increases with bond maturity. This trend could indicate the presence of common volatility drivers.

Table 3: Correlation Matrix of Absolute Yield Changes

	3M				3Y				10Y			
	DE	US	JPY	UK	DE	US	JPY	UK	DE	US	JPY	UK
DE	1	0.39	0.20	0.24	1	0.54	0.22	0.56	1	0.61	0.17	0.69
US		1	0.13	0.24		1	0.21	0.48		1	0.22	0.56
JPY			1	0.11			1	0.13			1	0.19
UK				1				1				1

Note: This table exhibits the correlation coefficients between the absolute yield changes of the government bonds of Germany (DE), the United States (US), Japan (JPY), and the United Kingdom (UK). Specifically, the 3 month, 3 year, and 10 year maturities are considered for the time period January 1995 - March 2024.

4.2 Macroeconomic Variables

In literature on country factors, domestic macroeconomic indicators are proven to interact and evolve dynamically with the extracted latent factors (see e.g. Ang and Piazzesi (2003) and Diebold et al. (2006)). The level and slope factor are particularly shown to be related with inflation and real activity measures, respectively. Consequently, Diebold et al. (2008) investigates these relationships on a global perspective. Additionally, Abbritti et al. (2013) and Byrne et al. (2019) propose additional variables to explain the behaviour of the global level factor, specifically international trade activity and global uncertainty.

In this section, I introduce the macroeconomic variables used for a correlation analysis, which aims to link the theoretical findings with real-world conditions. In particular, I consider a set of macroeconomic variables available from OECD.[1] The monthly observations of Harmonised Index of Consumer Prices (HICP), Composite Leading Indicator (CLI), Business Leading Indicator (BCI), and Unemployment Rate are considered. For the G-7 annual GDP growth, the G-7 and OECD inflation forecasts based on the Consumer Prices Index and Harmonised Index of Consumer prices, quarterly data is used. In addition, I use the monthly observations of the Economic Policy Uncertainty (EPU) indices of Baker et al. (2016). Except for the EPU index, which ranges from January 1997 - March 2024 due to data availability, all variable samples are from January 1995 - March 2024 (Q1 1995 - Q1 2024).

Figure 2 displays the standardized macroeconomic variables over time. Panels 2a and 2b show monthly observations, while Panel 2c plots quarterly data. The variables CLI, CCI, and BCI, presented in Panel 2a exhibit a high degree of co-movement, with negative spikes during the Great Financial Crisis and COVID-19 Crisis. When considering Panel 2b, we observe a peak in the unemployment rate during the previously mentioned crises, contrary to the one-year CPI growth rate, which exhibits roughly the same pattern as the variables in Panel 2a. Lastly, the variables in Panel 2c also shows signs of co-movement up to 2020, where the annual GDP growth spikes negatively. On the contrary, the OECD and G-7 one-year

[1]The macroeconomic variables are available at https://data-explorer.oecd.org/

inflation point forecasts peak in 2022.

Figure 2: Standardized Macroeconomic Variables

(a) CLI, CCI, and BCI

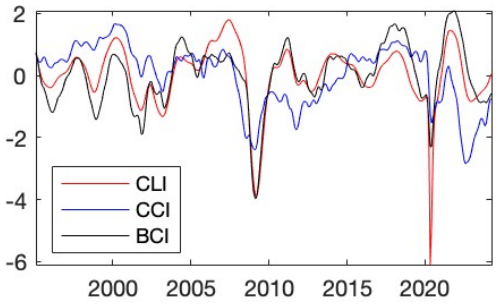

(b) Unemployment Rate, CPI, and EPU

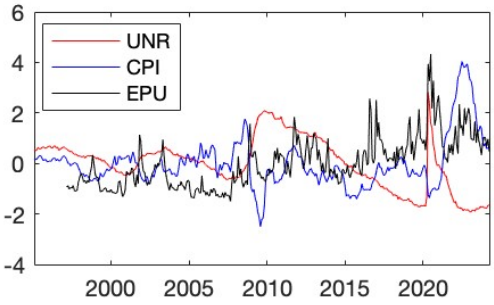

(c) GDP and Expected Inflation

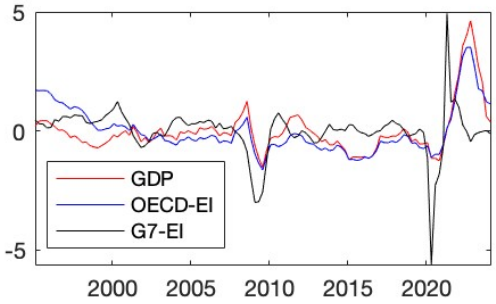

Note: Figure (a) plots the Composite Leading Indicator (CLI), Consumer Confidence Index (CCI), and Business Confidence Index (BCI) over time. Figure (b) plots the G-7 GDP-weighted unemployment rate (UR), the G-7 GDP-weighted one-year growth rate of the (Harmonised) Consumer Price Indices (CPI), and the G-7 GDP-weighted Economic Policy Uncertainty (EPU). Figure (c) plots the G-7 GDP weighted annual GDP growth, the OECD expected inflation (OECD-EI), and the G-7 GDP weighted expected inflation (G7-EI). Due to data availability, the EPU sample period is from January 1997 to March 2024, while the sample period for the other variables is from January 1995 to March 2024 with quarterly observations in figure (c). For comparison, all variables are standardized.

5 Empirical Results

This chapter describes the empirical results of the Gibbs sampler estimation. In section 5.1, I present the extracted global factors in combination with their underlying volatility processes. Section 5.2 links the theoretical results to the macroeconomy, while section 5.3 explains the results related to the country-specific factors. Section 5.4 exhibits the findings of the variance decompositions and section 5.5 ends with goodness of fit tests.

5.1 Global Factors

The Gibbs sampler is run using $S = 40{,}000$ iterations, of which the first $S_0 = 20,000$ iterations are discarded.[2] Figure 3 plots the posterior mean of the estimated latent global factors,

[2]For simulation exercises with more than 40,000 iterations, the results remain the same.

along with their posterior two standard deviation bands. The decay factor λ is constant over time for each country, and fixed at $\lambda = 0.0609$ following Diebold et al. (2008). The value of this decay factor maximizes the curvature loadings for the 2- and 3-year maturities, and thus fits the data. The narrow confidence interval suggests that the global factors are estimated with a high degree of precision, indicating clear convergence. The figure, in combination with Table 4, shows strong evidence of high persistence in the global factors, which signals model reliability and enhances economic interpretation and predictability. In addition, due to the identification of the country factor loadings, the scale of the global factors is not relevant.

Panel 3a displays the global level factor, which has a clear downward trend up to 2020, indicating the interest paid on bonds lowered globally. The steep decline of the factor from 1996 to 1999 is potentially caused by a combination of the Asian Financial Crisis in 1997 and the Russian Financial crisis in 1998. These crises increased global uncertainty, resulting in investors 'flight' to safer assets, government bonds. Furthermore, the global level factor increases from 2021 onwards, explained by the monetary tightening actions of the Federal Reserve (Fed), Bank of England (BoE), and the European Central Bank (ECB) to combat surging inflation.

In Panel 3b the global slope factor is exhibited. Important to note is that a negative (positive) value of the factor indicates a positive (negative) slope of the yield curve. Estrella and Mishkin (1998) and Diebold et al. (2008) argue that flat yield curves often precede economic downturns as they signal low future interest rates. The findings are consistent with this observation. We identify a flat slope factor in 1998, 2001, 2008, and 2019, corresponding to the Asian and Russian Financial Crises, the recessions in Japan, the US, and Germany in the early 2000s, the Great Financial Crisis, and the COVID-19 Pandemic, respectively. If this pattern holds, it suggests a potential for an upcoming economic downturn.

Figure 3: Posterior Mean and Two Posterior Standard Deviation Band of the Global Factors

(a) Global Level Factor

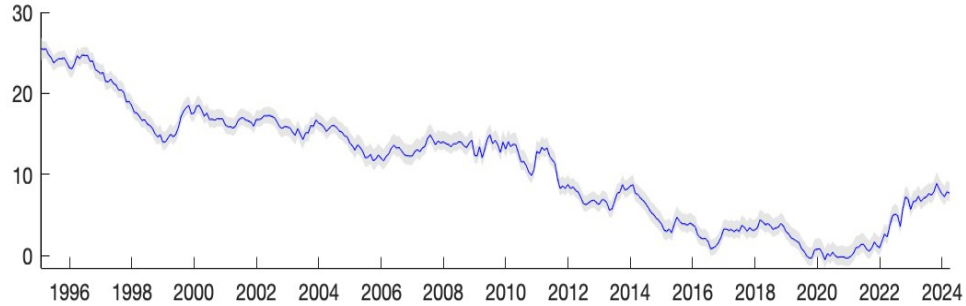

(b) Global Slope Factor

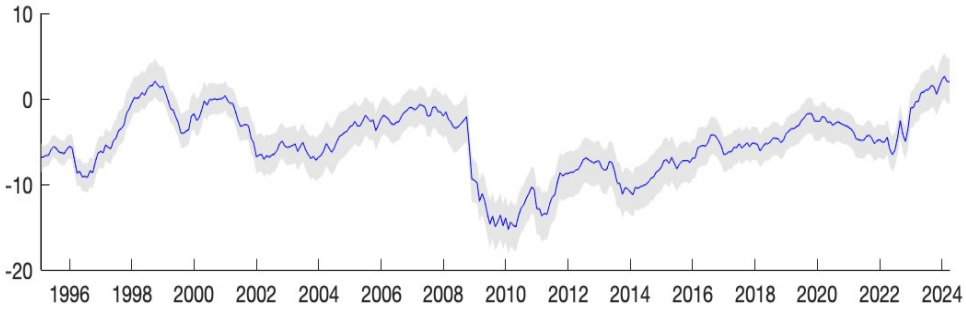

(c) Global Curvature Factor

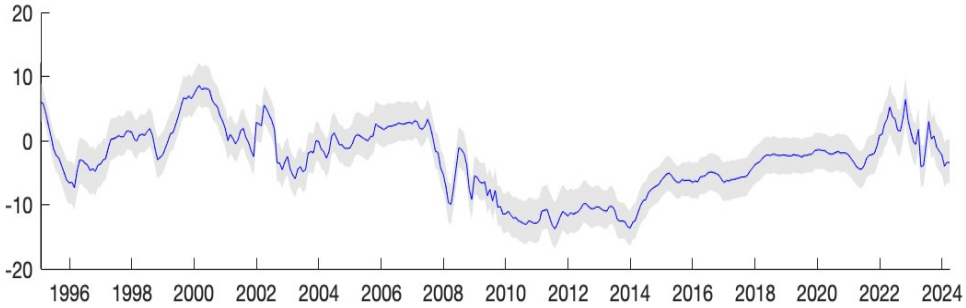

Note: The posterior draws of the global level, slope and curvature factor are obtained through the Carter and Kohn (1994) algorithm on the state space system presented in eq.(11) - (12). The posterior mean and posterior two standard deviation band are displayed for January 1995 - March 2024 for the decay factor $\lambda = 0.0609$.

Table 4: Estimates of the Coefficient Matrix Φ.

	L_{t-1}	S_{t-1}	C_{t-1}
L_t	0.988 (0.005)	0	0
S_t	0	0.981 (0.011)	0
C_t	0	0	0.957 (0.025)

Note: This table reports the posterior mean of the diagonal elements of the coefficient matrix Φ. In addition, the standard errors are shown in brackets below the estimates.

The interpretation of the global curvature factor, shown in Panel 3c, is a bit more tricky compared to the previous two factors. Diebold and Li (2006) show that the factor can be created as a summation of yields defined as $[y_t(24) - y_t(3)] - [y_t(120) - y_t(24)]$, assuming the decay factor $\lambda = 0.0609$. This fixed λ-value across countries and time means that the global curvature factor mostly influences the 2- and 3-year maturities. Intuitively, a positive

curvature factor indicates a more concave yield curve or even a humped yield curve, while a negative curvature factor suggest a less concave or convex yield curve. Abbritti et al. (2013) argues that peaks in the (global) curvature factor precede economic downturns. However, the presented figure does not show significant evidence to support the findings of Abbritti et al. (2013).

Table 5 presents the (mean) estimates of the coefficient matrix π, together with the mean of the stochastic volatility processes h_t, and the standard deviation of their error terms. The estimates show significant evidence for high autocorrelation in the factor volatilities. The interpretation of the mean of these processes is less relevant as it is dependent on initialization and identification methods.

Table 5: Coefficient Estimates of the Transition Equation of the Stochastic Volatility Processes h_t

Dynamics of the stochastic volatility processes h_t								
h_t^L	$=$	-1.049 (0.074)	$+$	0.963 (0.011)	$\tilde{h}_{t-1}^L +$	0.056 (0.003)	ξ_t^L
h_t^S	$=$	-0.623 (0.118)	$+$	0.933 (0.022)	$\tilde{h}_{t-1}^S +$	0.055 (0.003)	ξ_t^S
h_t^C	$=$	0.295 (0.144)	$+$	0.925 (0.025)	$\tilde{h}_{t-1}^C +$	0.056 (0.004)	ξ_t^C

Note: This table reports the posterior mean of the estimated stochastic volatility processes μ_h, the posterior mean of the diagonal elements of the coefficient matrix π, and the posterior mean of the error terms of the stochastic volatility processes h_t. In addition, the standard errors are shown in brackets below the estimates. Furthermore, I define $\tilde{h}_{t-1}^F \equiv (h_{t-1}^F - \mu_{h^F})$ for $F = L, S, C$.

Figure 4 plots the posterior mean of latent global factor volatility processes e^{h_t}, along with their two posterior standard deviation bands. These plots highlight the importance of accounting for time-varying volatility in the global factors. In particular, Panel 4a illustrates the volatility associated with the level of global bond yields. The level volatility peaks during 2008-2012, with the first peak coinciding with the Great Financial Crisis, during which central banks implemented monetary stimulus policies to support the economies. The second peak is likely due to the European Sovereign Debt crisis, causing investors to seek safer assets. Additionally, we observe a sharp increase in 2023, corresponding with global inflation surges and the monetary tightening measures to combat these issues. Overall, the volatility related to the level factor is relatively stable and low, partly contradicting the findings of Hautsch and Yang (2012), who find high volatility in times of high yields in the US.

Panel 4b shows the global slope volatility. We observe a peak in late 2008 to early 2009, while the impact of the European Debt Crisis in 2011-2012 seems to affect the slope volatility less significantly. This suggests that during the European Debt Crisis, the overall level of yields shifted, but the slope of their curves changed only slightly. Additionally, the impact of the inflation surges in 2022-2023 and the accompanying central bank policies are

Figure 4: Posterior Mean and Two Posterior Standard Deviation Band of the Stochastic Volatility Processes e^{h^F}

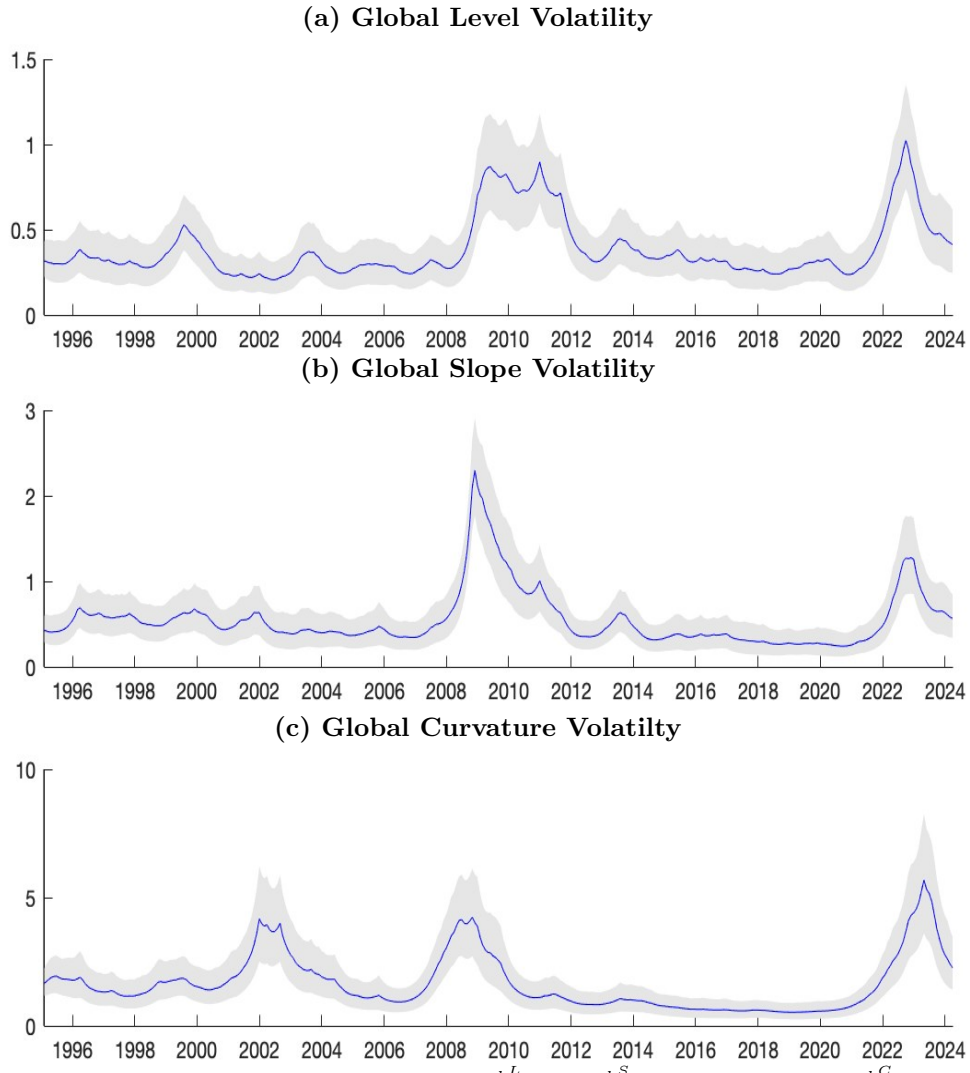

Note: The posterior draws of the global level volatility e^{h^L}, slope e^{h^S}, and curvature factor e^{h^C} are obtained through the Carter and Kohn (1994) algorithm applied on the state space system presented in eq.(18) - (19). The posterior mean and posterior two standard deviation band are displayed for January 1995 - March 2024.

clearly visible. Interestingly, slope volatility did not react as strongly to the central banks' monetary tightening measures to combat the recent inflation surge as it did to the stimulus measures during the Great Financial Crisis. The opposite seems to hold for the level factor. This could indicate that slope volatility is more influenced by monetary tightening, while level volatility is more affected by stimulus measures. This relationship requires further examination, which is beyond the scope of this paper.

The curvature volatility, shown in Panel 4c, exhibits a spike from late 2001 to late 2002. This spike is potentially linked to the aftermath of the Dot-Com Bubble Burst, which resulted in recessions in Japan, the US and Germany. Additionally, we observe peaks in 2008 and 2023, while there is no significant disturbance in mid-maturity yields during the European Debt Crisis.

5.2 Macroeconomic Links

One of the goals of this paper is to identify the macroeconomic forces driving government bond yields. The literature highlights significant co-movement between the global level factor and (expected) inflation. Specifically, Diebold et al. (2008) reports a correlation of 0.75 between G-7 inflation and the global level factor, while Abbritti et al. (2013) finds a 0.94 correlation between expected inflation of the OECD countries and their global level factor.[3] In addition, Byrne et al. (2019) finds that adding US and European sentiment and economic uncertainty measures to the regression of the global level factor on global macrofactors increases the models' explanatory power by more than 50%. Furthermore, the slope factor is often found to exhibit co-movement with the real activity. In Abbritti et al. (2013), the correlation between a proxy for the G-7 real activity and the slope factor is 0.74. On the other hand, Diebold et al. (2008) finds only a 0.27 correlation between the annual G-7 GDP growth and the slope factor.

Table 6: Correlation Coefficients with the Global Level Factor

	Level	
	Jan 1995: Sept 2008	Oct 2008 : March 2024
HICP	-0.07	-0.01
OECD-EI	0.87	-0.04
G7-EI	-0.11	0.09
CCI	0.19	-0.48
BCI	-0.21	-0.37
EPU	-0.09	-0.51

Note: This table presents the correlation coefficients between the extracted global level factor and a set of macroeconomic variables for two subsamples. Here, the abbreviations for the macroeconomic variables are HICP = Harmonised Index of Consumer Prices, OECDEI = OECD Expected Inflation, G7-EI = G-7 Expected Inflation, CCI = Consumer Confidence Index, BCI = Business Confidence Index, and EPU = Economic Policy Uncertainty.

Figure 5: Time Series of the Global Level Factor, and the OECD Inflation Forecast

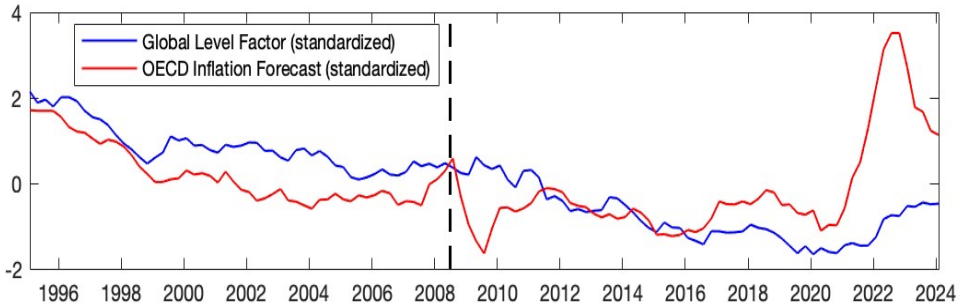

Note: This figure plots the posterior mean of the global level factor, together with the OECD one-year inflation forecast. Both time-series are standardized to illustrate the correlation. The sample consists of quarterly data ranging from 1995Q1 - 2024Q1, and splits in September 2008..

Table 6 displays the correlation coefficients between the macroeconomic variables

[3] Abbritti et al. (2013) consider the yield data of Japan, Canada, Switzerland, Germany, Australia, New Zealand, and the UK.

and the extracted global level factor. Contrary to the findings of Diebold et al. (2008), the correlation between the global level factor and the G-7 inflation measure, for which I use the one-year growth rate of the G-7 Harmonised Indices of Consumer Prices, is close to zero. For expected inflation, I consider two measures: the OECD one-year ahead inflation point forecast, and the first principal component of a matrix containing the one-year ahead inflation point forecasts for the G-7 countries. Both measures are quarterly data, so I only use the level factor for the closing month of each quarter. The OECD expected inflation, which can be viewed as a proxy for the world expected inflation, is highly correlated with the global factor in the first sub-sample, robust with the findings of Abbritti et al. (2013). However, as can be seen in Figure 5, this result radically changes for the second sub-sample. This change is potentially due to low central bank rates causing the level of the yield curves, especially the long-ends, to gradually decline, while expected inflation does not show this declining trend and is instead more volatile. Interestingly, the correlation between the G-7 expected inflation and the level factor is close to zero in the first subsample, indicating that the inflation and its expectation were relatively flat during that period. Concluding, these results highlight the reducing influence of inflation (expectations) on the level movements of the bond yields.

The economic policy uncertainty measure, for which I use the first principal component extracted from the matrix containing the economic policy uncertainty indices of the G-7 countries, has a correlation of -0.51 with the global level factor in the post-2008 period. Additionally, the sentiment measures are also negatively correlated with the factor in the second subsample. However, the correlation coefficients of the sentiment and policy measures are not sufficiently convincing to establish a clear relationship between these macroeconomic variables and the level factor.

Table 7: Correlation Coefficients with the Global Slope Factor

	Slope	
	Jan 1995: Sept 2008	Oct 2008 : March 2024
CLI	0.46	-0.01
GDPG	0.51	-0.04
UNR	-0.73	-0.77

Note: This table presents the correlation coefficients between the extracted global slope factor and a set of macroeconomic variables for two subsamples. Here, the abbreviations for the macroeconomic variables are CLI = Composite Leading Indicator, GDP = year-on-year quarterly Gross Domestic Product, UNR = G-7 GDP weighted Unemployment Rate.

Tabel 7 displays the correlations between the considered macroeconomic variables and the global slope factor. As indicators of the G-7 real activity, I consider the annual G-7 GDP growth, unemployment rate and Composite Leading Indicator (CLI). The unemploy-

Figure 6: Time Series of the Global Slope Factor and the G-7 Unemployment Rate

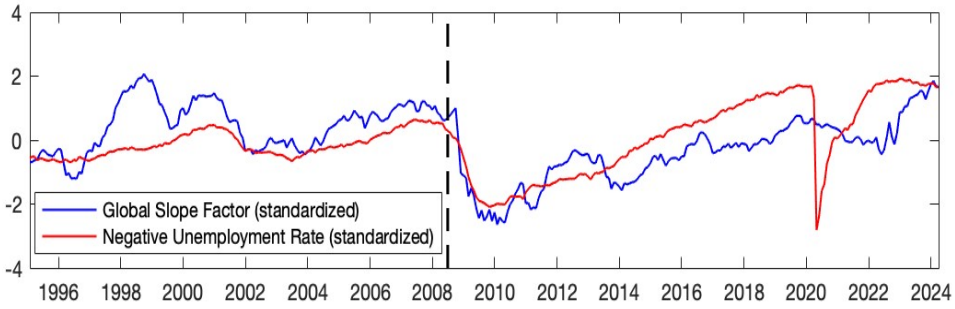

Note: This figure plots the posterior mean of the global slope factor, together with the negative G-7 unemployment rate. Both time-series are standardized to illustrate the correlation. The sample ranges from January 1995 till March 2024, and splits in September 2008.

ment rate is significant negatively correlated with the slope factor in the two subsamples, as highlighted in Figure 6. The figure highlights the co-movement between the two, briefly abrupted in 2020. Furthermore, the relationship between the slope factor and the GDP growth, and the CLI changes after the Great Financial Crisis.

The time-varying volatility in the level factor is used as a proxy of bond market volatility in Engle et al. (1990). Roughly at the same time, Merill Lynch introduced the Merrill Lynch Option Volatility Estimate (MOVE) Index (BofA, 1988). The index measures the implied volatility of US Treasury options. It considers options across a range of maturities, focusing on the 2-year, 5-year, 10-year, and 30-year Treasury bonds. I compute the monthly average of this index, available from November 2002, and correlate it with the stochastic volatility processes e^{h_t}. Figure 7 plots the MOVE index alongside the curvature volatility process $e^{h_t^C}$. The two time series have a correlation of 0.81. In comparison, the slope volatility shares a correlation of 0.77 with the MOVE index, whereas the global level volatility shows a correlation of only 0.52. This result indicates that the volatility in the US bond market co-moves with portfolios constructed with mid-term global bonds.

Lips (2012) models the time-varying volatility in US yields using a two-component GARCH specification and finds a link between the time-varying volatility component and the VIX, the Chicago Board Options Exchange's Volatility Index. I construct a global stock market volatility proxy using the VIX, Volatility DAX Index, FTSE 100 Volatility Index, and Nikkei 225 Volatility Index, and find no evidence supporting co-movement with the stochastic volatility processes. This indicates that volatility in global stock markets and bond markets operate independently. Additionally, for further research, it would be interesting to use a proxy for the global bond market volatility and compare this with the obtained volatility processes. However, constructing such a proxy requires the availability of volatility indices for other major bond markets.

Figure 7: Time Series of the MOVE index, and Curvature Volatility Process $e^{h_t^C}$

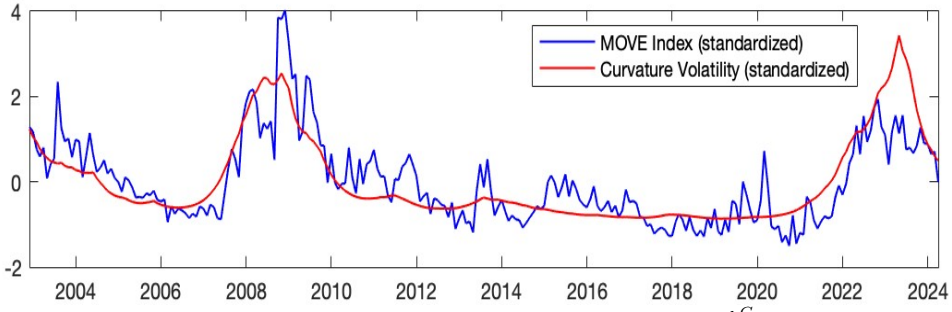

Note: This figures plots the posterior draws of the stochastic volatility process $e^{h_t^C}$, together with the Merill Lynch Option Volatility Estimate Index. Both time series are standardardized to illustrate the correlation. The sample ranges from November 2002 till March 2024, due to data availability on *Refinitiv*.

5.3 Country Factors

To assess the influence of using a one-step approach compared to the two-step estimation procedure of Diebold et al. (2008), I plot the obtained posterior means of the country factors against the same factors estimated through OLS. For the ease of the report, the figures are displayed in Appendix D. The one-step estimation method yields minimal differences for the level and slope factors, while we observe a greater degree of deviation in the curvature factors. The narrow posterior standard deviation bands of all country-specific factors, displayed in Appendix D, suggest a high degree of accuracy in the estimation method and indicate clear convergence. The remainder of this section discusses the estimation results related to the country factors.

Figure 8 displays the level, slope, and curvature factors for each country. The most noticeable aspect is the deviation of Japan's factors from those of other countries. The Bank of Japan's interest rates have been much less volatile historically. In 1999, the Bank of Japan introduced its Zero Interest Rate Policy, followed by a negative rate policy lasting until March 2024. The consistent monetary policy and infrequent rate changes have resulted in more stable yields on Japanese government bonds, which explains the deviation of the Japanese country factors. However, overall, the country factors show clear evidence of commonality in their dynamics. Performing PCA on each set of country factors confirms this observation, revealing that a principal component explains 86, 56, and 67 percent of the variances for the level, slope, and curvature factors, respectively. These findings align with and build upon those of Diebold et al. (2008), indicating that, with the inclusion of post-2008 data, there remains one dominant global level factor and one significant global slope factor. Additionally, the results reveal the presence of one significant global curvature factor.

Table 8 shows the estimates of the country factor loading equations and their idiosyncratic components $\alpha_{i,t}^f$. Overall, the high persistence in the idiosyncratic components

Figure 8: Posterior Mean of the Country Factors of Germany, the United States, the United Kingdom, and Japan

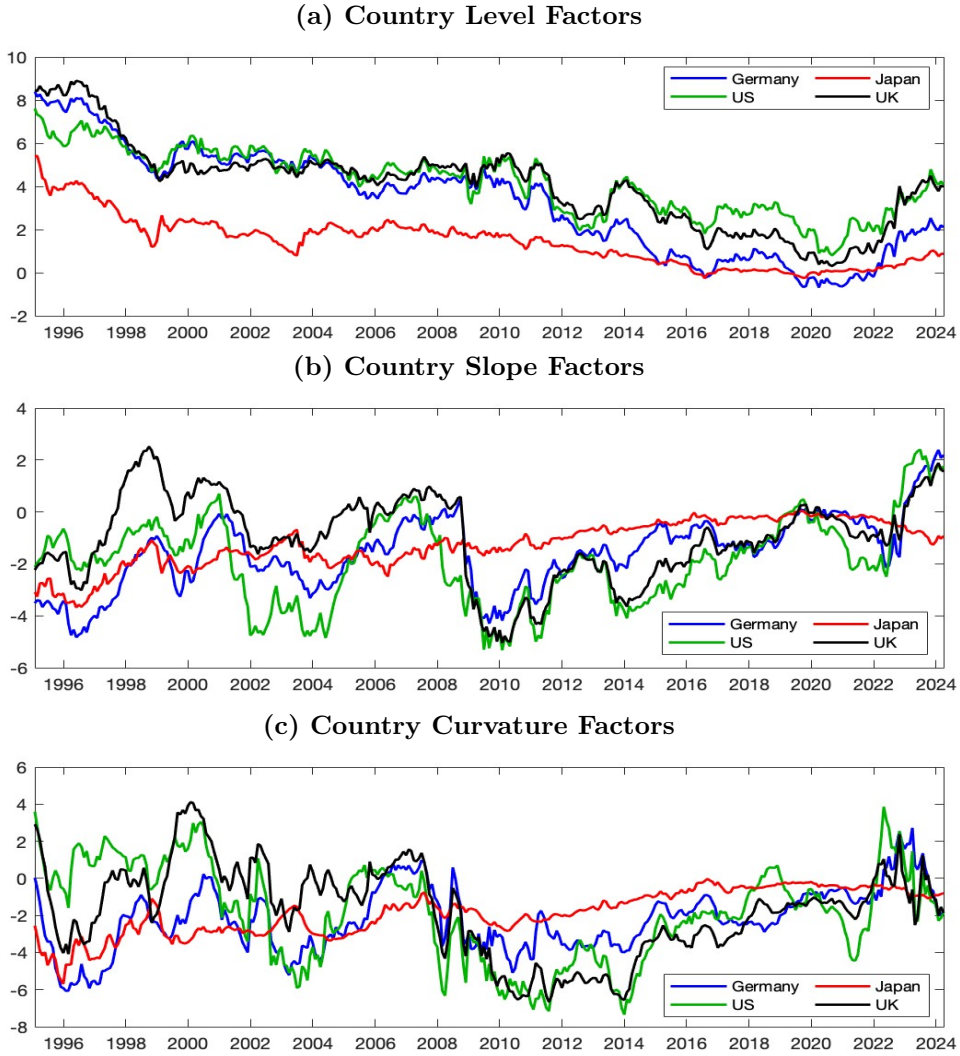

Note: The posterior draws of country factors $l_{i,t}$, $s_{i,t}$, and $c_{i,t}$ are obtained through the simplified version of the Kalman Filter applied on the state space system presented in eq.(**??** - (10). The posterior mean is displayed for January 1995 - March 2024.

highlights the significant influence of country-specific driving forces on the country factors, with only a few exceptions. The factor loadings of the country-level factors on the global level factors are estimated with high precision, as indicated by their significantly higher posterior means compared to their posterior standard deviations. Since the loadings are constrained to sum to one, they are relative to each other. The German level loading is the highest, and coupled with the relatively low persistence of its idiosyncratic component, this indicates that the German level factor aligns most closely with the global level factor. In contrast, the Japanese level loading is less than half that of its German counterpart and is the lowest among the four, which is consistent with my explanation of the Bank of Japan's policies.

The Japanese slope factor does not load on the global slope factor and is instead fully explained by its country-specific part. The UK slope loading is the highest among the four countries, followed by the US loading. Similar to the German level factor, the UK slope

Table 8: Parameter Estimates of the Country Factor Equations

Level Factors $l_{i,t}$									
$l_{GM,t}$	$= \alpha^l_{GM,t} +$	$\underset{(0.001)}{0.352} L_t +$	$\underset{(0.001)}{0.003} \tilde{e}_{GM,t},$	$\alpha^l_{GM,t} =$	$\underset{(0.219)}{-0.160} +$	$\underset{(0.427)}{0.672} \alpha^l_{GM,t-1} +$	$\underset{(0.001)}{0.004} \tilde{u}^l_{GM,t}$		
$l_{US,t}$	$= \alpha^l_{US,t} +$	$\underset{(0.001)}{0.210} L_t +$	$\underset{(0.004)}{0.021} \tilde{e}_{US,t},$	$\alpha^l_{US,t} =$	$\underset{(0.047)}{0.171} +$	$\underset{(0.024)}{0.910} \alpha^l_{US,t-1} +$	$\underset{(0.007)}{0.028} \tilde{u}^l_{US,t}$		
$l_{JP,t}$	$= \alpha^l_{JP,t} +$	$\underset{(0.001)}{0.158} L_t +$	$\underset{(0.002)}{0.007} \tilde{e}_{JP,t},$	$\alpha^l_{JP,t} =$	$\underset{(0.009)}{-0.022} +$	$\underset{(0.019)}{0.926} \alpha^l_{JP,t-1} +$	$\underset{(0.003)}{0.015} \tilde{u}^l_{JP,t}$		
$l_{UK,t}$	$= \alpha^l_{UK,t} +$	$\underset{(0.001)}{0.281} L_t +$	$\underset{(0.002)}{0.006} \tilde{e}_{UK,t},$	$\alpha^l_{UK,t} =$	$\underset{(0.011)}{0.021} +$	$\underset{(0.011)}{0.979} \alpha^l_{UK,t-1} +$	$\underset{(0.003)}{0.016} \tilde{u}^l_{UK,t}$		
Slope Factors $s_{i,t}$									
$s_{GM,t}$	$= \alpha^s_{GM,t} +$	$\underset{(0.017)}{0.228} S_t +$	$\underset{(0.003)}{0.010} \tilde{e}_{GM,t},$	$\alpha^s_{GM,t} =$	$\underset{(0.004)}{-0.005} +$	$\underset{(0.007)}{0.989} \alpha^s_{GM,t-1} +$	$\underset{(0.008)}{0.033} \tilde{u}^s_{GM,t}$		
$s_{US,t}$	$= \alpha^s_{US,t} +$	$\underset{(0.013)}{0.348} S_t +$	$\underset{(0.003)}{0.010} \tilde{e}_{US,t},$	$\alpha^s_{US,t} =$	$\underset{(0.012)}{-0.002} +$	$\underset{(0.016)}{0.975} \alpha^s_{US,t-1} +$	$\underset{(0.008)}{0.035} \tilde{u}^s_{US,t}$		
$s_{JP,t}$	$= \alpha^s_{JP,t} +$	$\underset{(0.009)}{0.007} S_t +$	$\underset{(0.003)}{0.014} \tilde{e}_{JP,t},$	$\alpha^s_{JP,t} =$	$\underset{(0.009)}{-0.018} +$	$\underset{(0.008)}{0.985} \alpha^s_{JP,t-1} +$	$\underset{(0.005)}{0.018} \tilde{u}^s_{JP,t}$		
$s_{UK,t}$	$= \alpha^s_{UK,t} +$	$\underset{(0.021)}{0.418} S_t +$	$\underset{(0.003)}{0.010} \tilde{e}_{UK,t},$	$\alpha^s_{UK,t} =$	$\underset{(0.050)}{0.171} +$	$\underset{(0.325)}{0.797} \alpha^s_{UK,t-1} +$	$\underset{(0.009)}{0.028} \tilde{u}^s_{UK,t}$		
Curvature Factors $c_{i,t}$									
$c_{GM,t}$	$= \alpha^c_{GM,t} +$	$\underset{(0.013)}{0.163} C_t +$	$\underset{(0.018)}{0.050} \tilde{e}_{GM,t},$	$\alpha^c_{GM,t} =$	$\underset{(0.027)}{-0.065} +$	$\underset{(0.015)}{0.962} \alpha^c_{GM,t-1} +$	$\underset{(0.030)}{0.170} \tilde{u}^c_{GM,t}$		
$c_{US,t}$	$= \alpha^c_{US,t} +$	$\underset{(0.017)}{0.392} C_t +$	$\underset{(0.020)}{0.067} \tilde{e}_{US,t},$	$\alpha^c_{US,t} =$	$\underset{(0.021)}{-0.024} +$	$\underset{(0.015)}{0.962} \alpha^c_{US,t-1} +$	$\underset{(0.027)}{0.121} \tilde{u}^c_{US,t}$		
$c_{JP,t}$	$= \alpha^c_{JP,t} +$	$\underset{(0.001)}{0.001} C_t +$	$\underset{(0.007)}{0.018} \tilde{e}_{JP,t},$	$\alpha^c_{JP,t} =$	$\underset{(0.019)}{-0.039} +$	$\underset{(0.010)}{0.979} \alpha^c_{JP,t-1} +$	$\underset{(0.017)}{0.050} \tilde{u}^c_{JP,t}$		
$c_{UK,t}$	$= \alpha^c_{UK,t} +$	$\underset{(0.015)}{0.444} C_t +$	$\underset{(0.017)}{0.054} \tilde{e}_{UK,t},$	$\alpha^c_{UK,t} =$	$\underset{(0.029)}{-0.038} +$	$\underset{(0.071)}{0.866} \alpha^c_{UK,t-1} +$	$\underset{(0.037)}{0.142} \tilde{u}^c_{UK,t}$		

Note: This table reports the Bayesian estimates of the global model from January 1995 - March 2024 given by eq. (3) - (4). The posterior standard deviations are reported in parenthesis. I define $\tilde{e}^f_{i,t} \equiv e^f_{i,t}/\sigma_{e^f_i}$ and $\tilde{u}^f_{i,t} \equiv u^f_{i,t}/\sigma_{u^f_i}$, such that $e^f_{i,t} \equiv \sigma_{e^f_i} \tilde{e}^f_{i,t}$ and $u^f_{i,t} \equiv \sigma_{e^f_i} \tilde{e}^f_{i,t}$. For more details, consider the text.

factor's idiosyncratic component has a relative low persistence and high standard deviation, indicating that the UK slope factor closely matches the global slope factor. Additionally, the German slope loading loads on the global yield slope. This differs from the findings of Diebold et al. (2008), where the German slope loading was found to be insignificant. This contradicting finding suggests that the dynamics have shifted over the last fifteen years. Furthermore, the estimates of the country-specific curvature factor equations exhibit roughly the same results as those of the slope factors; the Japanese curvature factor is fully explained by its country-specific part, and the UK yield curvature matches the global curvature factor most closely.

To analyze the behavior of the country-specific factors compared to the common forces more closely, I plot the dynamics of the idiosyncratic components $\alpha^f_{i,t}$ in Figure 9. These plots show how the country-specific factors deviate from their respective global factors and highlight the importance of implementing time-varying idiosyncratic components. The German level component is relatively flat, confirming that its level factor closely resembles the global factor. Additionally, we observe contrasting movements in the level components of Japan and the US in late 2012 and 2020. The flight to safety (from Japan to the US)

Figure 9: Posterior Mean of the Idiosyncratic Components of Germany, the United States, the United Kingdom, and Japan across Time

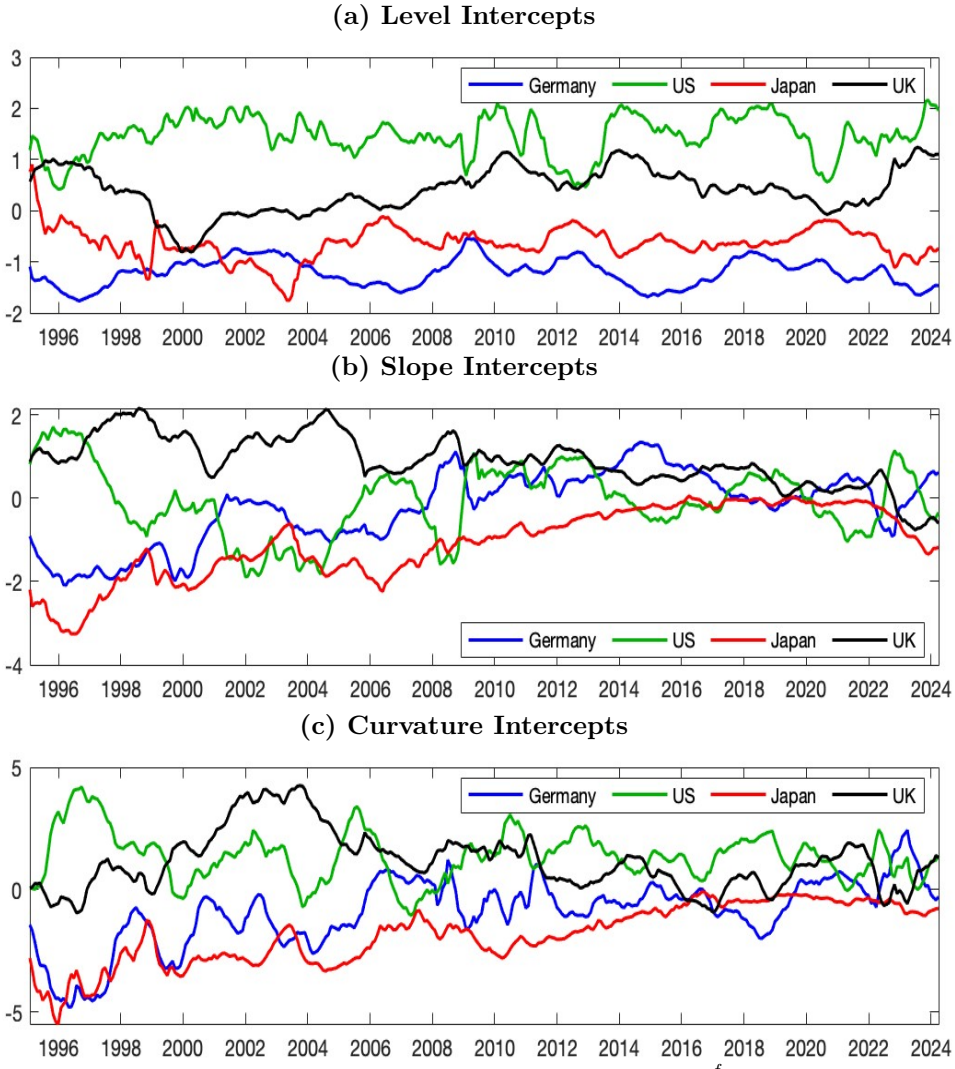

Note: The figure presents the posterior draws of idiosyncratic components $\alpha_{i,t}^{f}$ for each country, obtained through the Carter and Kohn (1994) algorithm applied on the state-space system presented in eq.(13) - (14). The posterior mean is displayed for January 1995 - March 2024.

at the end of 2012 is potentially linked to the political shift in Japan following the election of Shinzo Abe, combined with the announcement of a quantitative easing round in the US. Conversely, the pattern in 2020 can be explained by the COVID-19 pandemic, which resulted in the Federal Reserve cutting rates to near zero and launching quantitative easing programs.

The slope and curvature time-varying intercepts, displayed in Panel 9b and Panel 9c, exhibit less volatile behavior in the post-2008 period. This convergence suggests that the slope and curvature factors for the US, UK, and Germany closely match their global counterparts, potentially due to similar policy measures by their central banks. However, for the German and US slope components, we observe counter-cyclical movements from 2012 until the end of the sample. These movements indicate that post-2008, a flattening of the US yield curve pairs with a steepening of the German yield curve, and vice versa. This relationship could

be explained by changing investor preferences in short-term sovereign bonds.

5.4 Variance Decomposition

By using the one-step estimation approach combined with time-varying intercepts $\alpha_{i,t}^{f}$ and stochastic volatility in the global error terms η_t, the construction of the country-specific factors differs from that in Diebold et al. (2008). These changes affect the explanatory power of common forces on the variance of the country-specific factors. In this section, I decompose the variance of the country-specific factors into portions driven by the common component and the idiosyncratic components. The time-varying nature of the global factors' variance allows for an investigation of the dynamics of this decomposition over time. Specifically, to identify the sources of uncertainty, I consider the short-term forecast error, given by

$$V[f_{i,t+1}] = V[\alpha_{i,t+1}^{f}] + (\beta_i^f)^2 V[F_{t+1}] + V[e_{i,t+1}^{f}] = \sigma^2_{u_i^f} + (\beta_i^f)^2 \omega_t^F + \sigma^2_{e_i^f}, \tag{23}$$

where ω_t^F is the diagonal element of Ω_t corresponding with country factor f, for $f = l, s, c$. The idiosyncratic part of the decomposition is given by $\sigma^2_{u_i^f} + \sigma^2_{e_i^f}$, while $(\beta_i^f)^2 \omega_t^F$ represents the common part. Note that the decomposition is possible because the disturbances are mutually uncorrelated in this model.

Figure 10 displays the common component of the one-month-ahead forecast error variances as a percentage. At first glance, the uncertainty in the country-specific factors driven by the common forces shows strong co-movement with the stochastic volatility processes in these forces. Given the time-invariance of the idiosyncratic variance and factor loadings, this result is logical. Interestingly, the percentage of uncertainty in the level factors explained by the common component is, over the entire sample period, lower for each country compared to Diebold et al. (2008). This result suggests that the idiosyncratic forces driving country factors have increased since 2008. Furthermore, Panel 10a accentuates the dependence of the German level factor on the global factor.

The uncertainty in the UK slope factor is primarily explained by the global slope factor, highlighting the strong co-movement between the two. Furthermore, although the German slope loading is lower than its US counterpart, it is more influenced by uncertainty in the common force. This indicates that the idiosyncratic variance of the US is higher than that of Germany, suggesting greater movement in the US yield curve slope compared to Germany. Furthermore, the results of the country factor variance decomposition of the slope and curvature factors show the divergence of the Japanese curvature factor with its global

Figure 10: One-Month-Ahead Forecast Error Variance

(a) Level Uncertainty

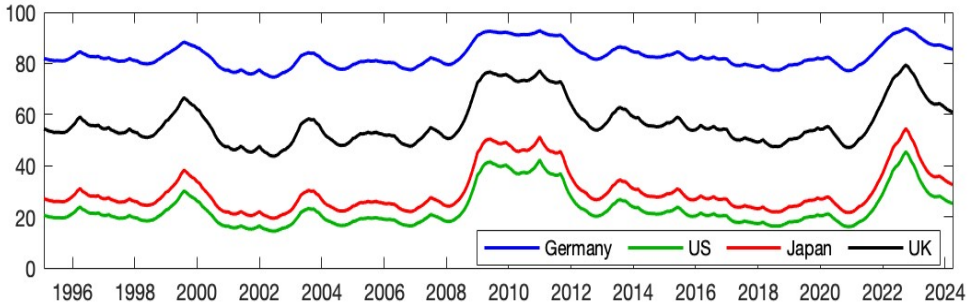

(b) Slope Uncertainty

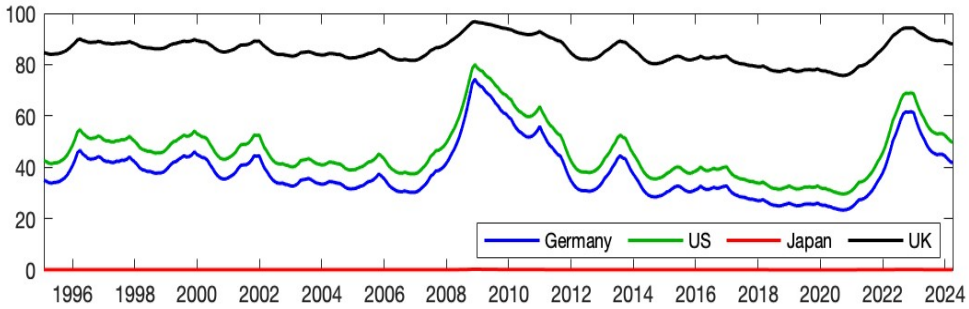

(c) Curvature Uncertainty

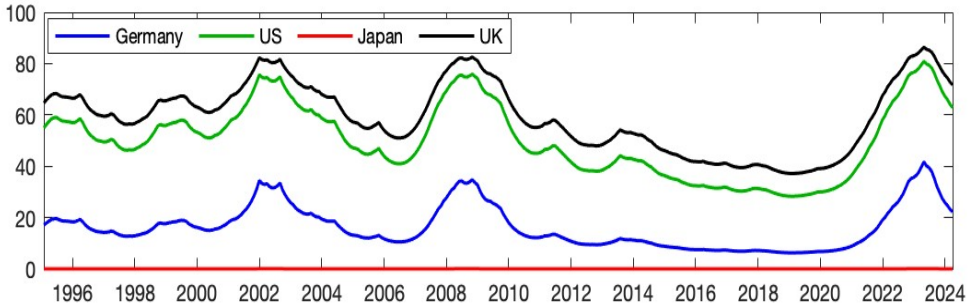

Note: This figure displays the percentage of variance that is explained by the common component part for each country factor $f_{i,t}$. The variance of the posterior mean of the country-specific factors $f_{i,t}$ is decomposed into a idiosyncratic part $\sigma^2_{u_i^f} + \sigma^2_{e_i^f}$ and a common component part $(\beta_i^f)^2\omega_t^F$. The posterior mean is displayed for January 1995 - March 2024.

counterpart. Additionally, the global curvature factor accounts for between 40-80 percent of the US and UK curvature factors during the sample period. Contrary to Germany, where this percentage is between 10-40 percent which confirms the higher idiosyncratic dependence in the German curvature factor earlier found.

5.5 Goodness of Fit

To assess the goodness of fit of the model, I perform two sets of tests. For the first test, I follow Diebold and Li (2006), who evaluate the model's ability to capture various yield curve shapes and accurately fit actual yields. Specifically, I compute the fitted yield curves as a function of maturity and compare these to the actual yield curves. Figure 11 illustrates the

model-implied fitted curves for each country on three different dates, selected to showcase a variety of yield curve shapes. Examination reveals the model's proficiency in replicating concave, inverted, and even inverted-humped yield curves. Except for the curve on 1 May 2008 in Germany, the model closely aligns with the actual yield curves.

Figure 11: Fitted Yield Curves Compared to Actual Yield Curves

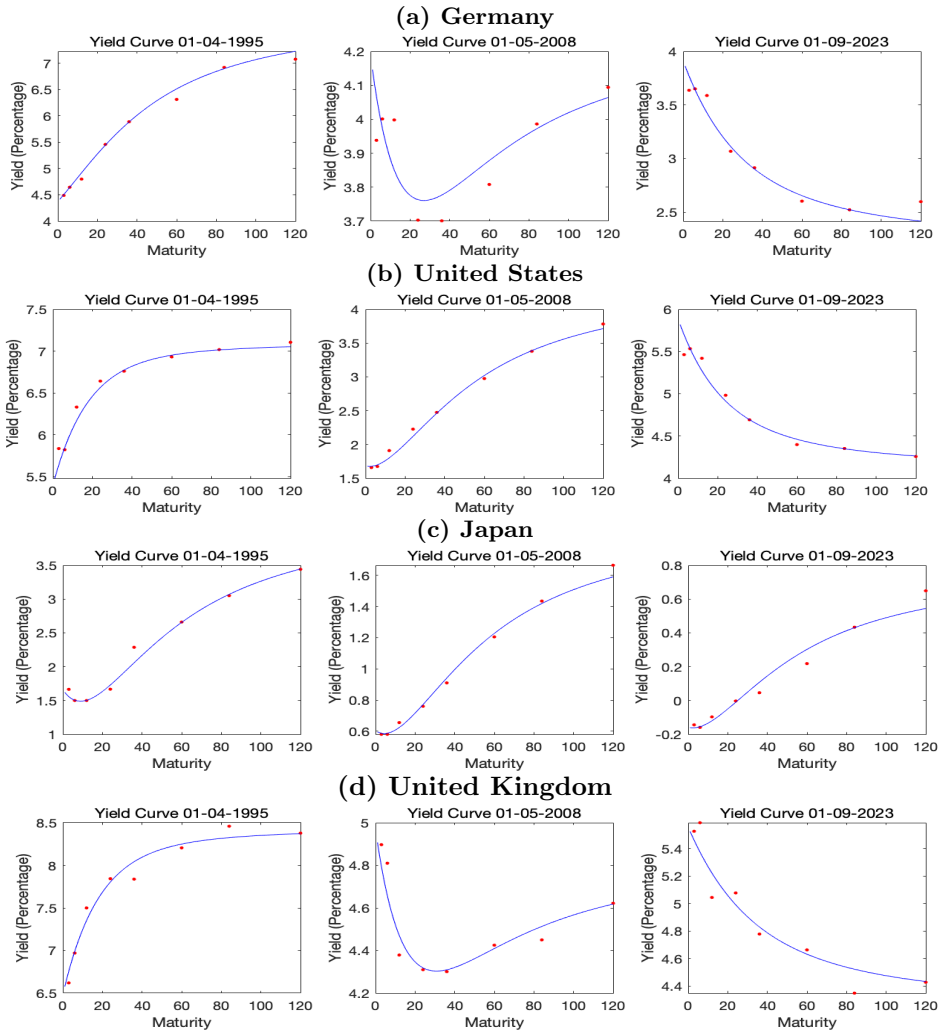

Note: This figure plots the model-implied fitted yield curves using the mean of the posterior country factor draws, together with the actual yield curves. For each country, exhibited by a panel, three dates are presented to assess to goodness of fit of the HSV-DNS model.

The second fit assessment aims to evaluate the models' proficiency to reproduce data characteristics and the improvement in model fit when incorporating stochastic volatility in the global factors error terms. Meng (1994) introduces posterior predictive p-values (ppp-values), an evaluation method of the models' fit for Bayesian frameworks. The idea behind the approach is to generate N draws of the data series y_t^{gen} and to compute the probability that a generated series is more extreme than the actual observed data y_t^{act}. Intuitively, if the data fits the model well, the generated data series should be close to the actual data, resulting in high ppp-values. More specifically, Chan et al. (2019) show that the ppp-value

can be calculated as the relative amount of draws that exceed the actual data, which gives

$$ppp = \mathrm{P}[g(y_t^{gen}) \geq g(y_t^{act})] = \frac{1}{N}\sum_{i=1}^{N} \mathrm{I}\left[g(y_t^{gen(i)}) \geq g(y_t^{act})\right], \tag{24}$$

where I[·] is the indicator function. Furthermore, $g(\cdot)$ denotes a function, which is usually chosen as a sample statistic. In this case, the pricing errors $v_t(\tau_j)$ of the yield data are assumed to be normally distributed. Therefore, I choose $g(.)$ as $\mathbb{E}[V|y^x]$ and $\mathbb{E}[Skew|y^x]$, where V denotes the sample variance and $Skew$ the sample skewness and y^x can be y_t^{gen} or y_t^{act}.

Using the draws after the burn-in period from the Gibbs Sampler, I generate $N = 20,000$ series of yield data y_t^{gen} from

$$p(y_t^{gen(i)}|f_t^{(i)}, \Sigma_v^{(i)}) \sim \mathrm{N}(\Pi(\lambda)f_t^{(i)}, \Sigma_v^{(i)}), \tag{25}$$

where $\Pi(\lambda)$ is the matrix containing the country factor loadings, and $f_t^{(i)}$ and $\Sigma_v^{(i)}$ represent the i-th draw of country factors and the yield pricing error covariance matrix, respectively. Then, to calculate the sample variance and skewness, I compute the error terms for each draw as $v_t^{gen(i)} = y_t^{gen(i)} - \Pi(\lambda)f_t^{(i)}$ and $v_t^{act(i)} = y_t^{act} - \Pi(\lambda)f_t^{(i)}$. The threshold $g(y_t^{act})$ is then produced by taking the average of the considered sample statistic of all $v_t^{act(i)}$ draws. Consequently, the ppp-values can be calculated using eq.(25).

Table 9 shows the ppp-values for the HSV-DNS model and the same model that assumes the global factor error terms η_t to have a constant variance, denoted as the Hierachical dynamic Nelson-Siegel (HDNS) model. With the exception of the 10-year Treasury and the 1-year Japanese bond, both models are likely to generate yield series data that have more extreme properties than the actual data, highlighted by the high *ppp*-values. This result further emphasizes the model's proficiency in capturing the data's characteristics. Furthermore, when comparing the HSV-DNS model and the HDNS model, we observe minimal differences in model fit. This observation indicates that the estimation of the country factors is not strongly dependent on the stochastic volatility processes of the global factors. Additionally, the pricing error terms $v_t(\tau_j)$ exhibit non-Gaussian skewness. To further examine, I plot the pricing error terms $v_t(\tau_j)$ of the HSV-DNS model in Figure 12. The figure highlights the influence of outliers on the skewness of the error terms, for example in the German 3-month Bund. Furthermore, the plots show the model's weak ability to correctly price the 10-year Treasury and Japanese bond. Overall, the model fit looks sufficient but shows the potential for improvement, which would be an interesting topic for further research.

Table 9: Posterior Predictive P-values

		HSV-DNS				HDNS			
		Variance		Skewness		Variance		Skewness	
	τ	$\mathbb{E}[V\|y_t^{act}]$	*ppp*	$\mathbb{E}[S\|y_t^{act}]$	*ppp*	$\mathbb{E}[V\|y_t^{act}]$	*ppp*	$\mathbb{E}[S\|y_t^{act}]$	*ppp*
DE	3M	0.009	0.999	-0.850	0.999	0.009	0.999	-0.829	0.999
	1Y	0.007	0.996	-0.297	0.989	0.007	0.995	-0.294	0.987
	5Y	0.006	0.999	-1.105	0.999	0.006	0.999	-1.126	0.999
	10Y	0.019	0.992	0.030	0.409	0.019	0.990	0.027	0.412
US	3M	0.027	0.659	-0.094	0.768	0.028	0.658	-0.095	0.772
	1Y	0.005	0.999	-0.030	0.596	0.005	0.999	-0.035	0.610
	5Y	0.002	0.998	-0.094	0.766	0.001	0.999	-0.094	0.766
	10Y	0.006	0.963	0.771	0.001	0.006	0.964	0.776	0.001
JPY	3M	0.004	0.976	-0.717	0.999	0.004	0.975	-0.724	0.999
	1Y	0.002	0.999	0.282	0.002	0.002	0.999	0.277	0.017
	5Y	0.003	0.999	-0.013	0.547	0.003	0.999	-0.019	0.561
	10Y	0.004	0.999	0.168	0.100	0.004	0.999	0.169	0.094
UK	3M	0.033	0.494	-1.645	0.999	0.035	0.507	-1.255	0.999
	1Y	0.002	0.484	-0.408	0.999	0.017	0.482	-0.359	0.997
	5Y	0.013	0.535	-0.222	0.959	0.013	0.527	-0.207	0.943
	10Y	0.002	0.455	0.006	0.480	0.001	0.455	0.001	0.490

Note: This table exhibits the posterior predictive p-values p of the Hierarchical Stochastic Volatility dynamic Nelson-Siegel model and the Hierarchical dynamic Nelson-Siegel model. The sample variance V and sample skewness S are chosen for the function $g(\cdot)$ in eq.(25).

Figure 12: Yield Pricing Errors

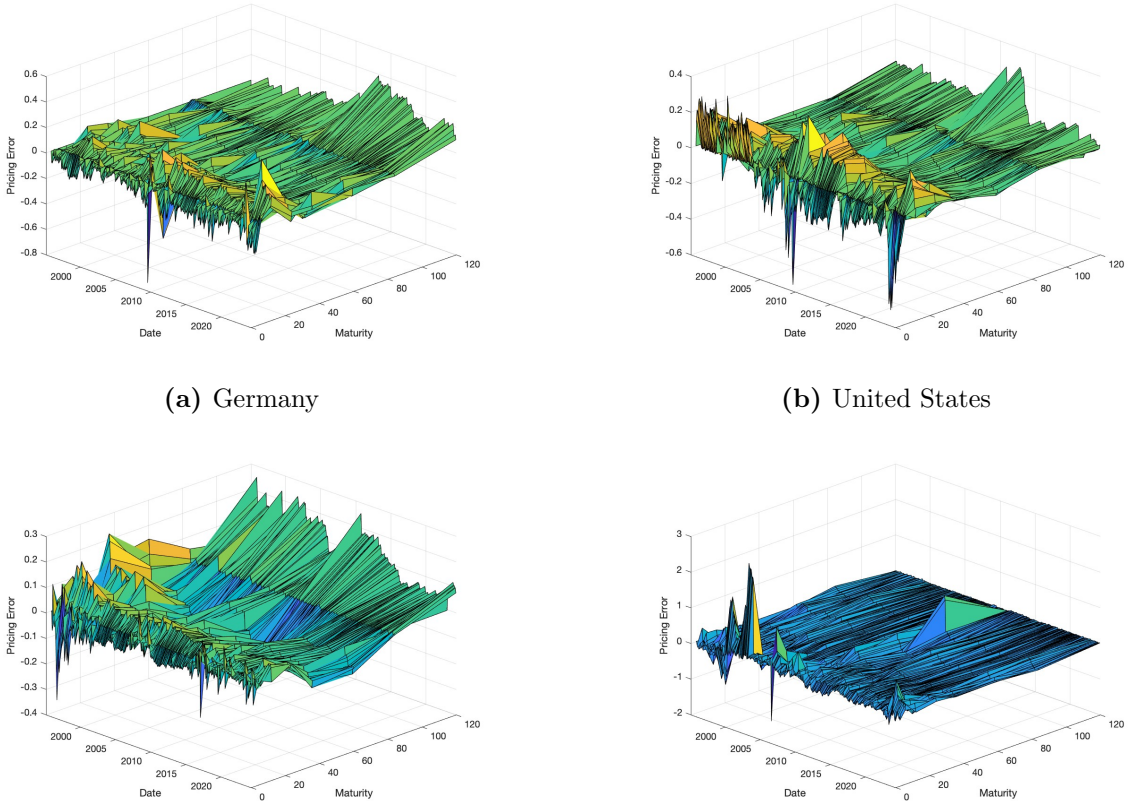

(a) Germany **(b)** United States

(c) Japan **(d)** United Kingdom

Note: These figures plot the pricing errors $v_t(\tau_j)$ of the HSV-DNS model across time and maturity for Germany, the United States, Japan, and the UK. The sample ranges from January 1995 till March 2024 and considers eight maturities.

6 Conclusion

In this paper, I extend the work on global yield factors by Diebold et al. (2008). Although existing literature often overlooks the time-varying volatility in global yield factors, understanding these dynamics is crucial, especially in the context of risk management policies. To address this gap, I employ a Hierarchical Stochastic Volatility dynamic Nelson-Siegel model, inspired by Tornese (2023) and incorporate the stochastic volatility framework of Hautsch and Yang (2012), to further explore how time-varying volatility in global factors influences global bond yields. Specifically, I consider the yields of German, US, Japanese, and UK government bonds from January 1995 till March 2024.

Utilizing the one-step Bayesian MCMC estimation method of Byrne et al. (2019) in combination with the stochastic volatility estimation technique of Hautsch and Yang (2012), I extract country-specific factors, global factors, and the stochastic volatility processes in the global factors out of the data. In my empirical study, I find strong evidence of time-varying volatility in the global factors. The stochastic processes are highly autocorrelated, seem to evolve dynamically, and take on large values in times of financial distress. The volatility process of the global curvature factor shows strong co-movement with the MOVE index, a US bond market proxy. Furthermore, when re-evaluating the global factors' connection to the macroeconomy, I find a drastic change in relationship between the global level factor and the expected inflation post-2008. Additionally, the global slope factor is heavily negatively correlated with the G-7 unemployment rate. The one-step estimation method that incorporates parameter uncertainty in all estimated parameters, yields small differences for the country level and slope factors compared to standard OLS estimates, and larger ones for the country curvature factors.

There are many opportunities for future research. To better understand the dynamics of global stochastic volatility processes driving bond markets, it would be valuable to further analyze their relationship with macroeconomic fundamentals and monetary policy channels. Additionally, with the increasing availability of daily yield data, modeling stochastic volatility in this context could be of interest to market practitioners. Comparing such volatility processes with, for example, interest rate derivative-implied volatility measures could yield valuable insights in bond markets' volatility. In terms of model improvement, there is a strong case to be made for the use of non-Gaussian error terms. Researching the influence of skewed and heavy-tailed error term distributions, along with the accommodating changes in estimation method, could further enhance the insights into the robustness of the results.

References

Abbritti, M., Dell'Erba, M., Moreno, M., & Sola, M. (2013). Global factors in the term structure of interest rates (no. 13-223). *International Monetary Fund. https://doi.org/10.5089/9781475513516.001*.

Ang, A., & Piazzesi, M. (2003). A no-arbitrage vector autoregression of term structure dynamics with macroeconomic and latent variables. *Journal of Monetary economics*, *50*(4), 745–787.

Baker, S. R., Bloom, N., & Davis, S. J. (2016). Measuring economic policy uncertainty. *The quarterly journal of economics*, *131*(4), 1593–1636.

BofA. (1988). Merrill lynch option volatility estimate (move) index [Retrieved from Refinitiv]. https://www.refinitiv.com

Byrne, J. P., Cao, S., & Korobilis, D. (2019). Decomposing global yield curve co-movement. *Journal of Banking & Finance*, *106*, 500–513.

Carter, C. K., & Kohn, R. (1994). On gibbs sampling for state space models. *Biometrika*, *81*(3), 541–553.

Casella, G., & George, E. I. (1992). Explaining the gibbs sampler. *The American Statistician*, *46*(3), 167–174.

Chan, J., Koop, G., Poirier, D. J., & Tobias, J. L. (2019). *Bayesian econometric methods* (Vol. 7). Cambridge University Press.

Cogley, T., & Sargent, T. J. (2005). Drifts and volatilities: Monetary policies and outcomes in the post wwii us. *Review of Economic dynamics*, *8*(2), 262–302.

Diebold, F. X., & Li, C. (2006). Forecasting the term structure of government bond yields. *Journal of econometrics*, *130*(2), 337–364.

Diebold, F. X., Li, C., & Yue, V. Z. (2008). Global yield curve dynamics and interactions: A dynamic nelson–siegel approach. *Journal of Econometrics*, *146*(2), 351–363.

Diebold, F. X., Rudebusch, G. D., & Aruoba, S. B. (2006). The macroeconomy and the yield curve: A dynamic latent factor approach. *Journal of econometrics*, *131*(1-2), 309–338.

Ding, Z., Granger, C. W., & Engle, R. F. (1993). A long memory property of stock market returns and a new model. *Journal of empirical finance*, *1*(1), 83–106.

Engle, R. F., Ng, V. K., & Rothschild, M. (1990). Asset pricing with a factor-arch covariance structure: Empirical estimates for treasury bills. *Journal of econometrics*, *45*(1-2), 213–237.

Estrella, A., & Mishkin, F. S. (1998). Predicting us recessions: Financial variables as leading indicators. *Review of Economics and Statistics*, *80*(1), 45–61.

Fuller, W. (1996). Introduction to statistical time series: Wayne a. fuller (1996): (2nd edition). wiley, isbn 0-471-55239-9, pp. 736, [pound sign] 55.00. *Computational Statistics Data Analysis*, *23*(1), 200–201. https://EconPapers.repec.org/RePEc:eee:csdana:v:23:y:1996:i:1:p:201-200a

Hautsch, N., & Ou, Y. (2008). Discrete-time stochastic volatility models and mcmc-based statistical inference. *Available at SSRN 1292494*.

Hautsch, N., & Yang, F. (2012). Bayesian inference in a stochastic volatility nelson–siegel model. *Computational Statistics & Data Analysis*, *56*(11), 3774–3792.

Jotikasthira, C., Le, A., & Lundblad, C. (2015). Why do term structures in different currencies co-move? *Journal of Financial Economics*, *115*(1), 58–83.

Kim, C.-J., Nelson, C. R., et al. (1999). State-space models with regime switching: Classical and gibbs-sampling approaches with applications. *MIT Press Books*, *1*.

Kim, S., Shephard, N., & Chib, S. (1998). Stochastic volatility: Likelihood inference and comparison with arch models. *The review of economic studies*, *65*(3), 361–393.

Koopman, S. J., Mallee, M. I., & Van der Wel, M. (2010). Analyzing the term structure of interest rates using the dynamic nelson–siegel model with time-varying parameters. *Journal of Business & Economic Statistics*, *28*(3), 329–343.

Lips, B. (2012). Time-varying volatility in the dynamic nelson-siegel model. *Quantitative Finance*.

Meng, X.-L. (1994). Posterior predictive p-values. *The annals of statistics*, *22*(3), 1142–1160.

Moench, E., Ng, S., & Potter, S. (2013). Dynamic hierarchical factor models. *Review of Economics and Statistics*, *95*(5), 1811–1817.

Mönch, E. (2012). Term structure surprises: The predictive content of curvature, level, and slope. *Journal of Applied Econometrics*, *27*(4), 574–602.

Nelson, C. R., & Siegel, A. F. (1987). Parsimonious modeling of yield curves. *Journal of business*, 473–489.

Primiceri, G. E. (2005). Time varying structural vector autoregressions and monetary policy. *The Review of Economic Studies*, *72*(3), 821–852.

Taylor, S. J. (2008). *Modelling financial time series*. world scientific.

Tornese, T. (2023). A euro area term structure model with time varying exposures. *BAFFI CAREFIN Centre Research Paper*, (199).

Waggoner, D. F. (1997). Spline methods for extracting interest rate curves from coupon bond prices. *Federal Reserve Bank of Atlanta Working Paper*, 97–10.

A Gibbs Sampler

To enhance readability, I define $\theta_{\text{-}}$ a the parameter set θ minus the sampled parameter at that particular step of the algorithm, and introduce $\Theta_{\text{-}} = \{y_t, \theta, f_t, \bar{F}_t, \alpha_t\}$. The full procedure of the Gibbs Sampler is as follows

1. Initialize Θ
2. Sample the variables in Θ from $\Theta|y_t$ using S replications, where the initial S_0 samples are discarded
   (a) Sample the variables θ from $p(\theta|y_t, f_t, Z_t, H)$
      i. Sample each diagonal element of Σ_v from $p(\sigma^2_{v_i}|y_t, \theta_{\text{-}}, f_t, \bar{F}_t, \alpha_t, H) \sim$ IG
      ii. Sample each diagonal element of Σ_e from $p(\sigma^2_{e_i^f}|y_t, \theta_{\text{-}}, f_t, \bar{F}_t, \alpha_t, H) \sim$ IG
      iii. Sample each diagonal element of Σ_u from $p(\sigma^2_{u_i^f}|y_t, \theta_{\text{-}}, f_t, \bar{F}_t, \alpha_t, H) \sim$ IG
      iv. Sample each element of B from $p(\beta_i^f|y_t, \theta_{\text{-}}, f_t, \bar{F}_t, \alpha_t, H) \sim$ N
      v. Sample each combination of C and Φ from $p(C^F, \phi^F|y_t, \theta_{\text{-}}, f_t, \bar{F}_t, \alpha_t, H) \sim$ N
      vi. Sample each combination of Γ and Ψ from $p(\gamma_i^f, \psi_i^f|y_t, \theta_{\text{-}}, f_t, \bar{F}_t, \alpha_t, H) \sim$ N
   (b) Sample the country factors f_t from $p(f_t|y_t, \theta, \bar{F}_t, \alpha_t, H)$ using a simplified Kalman filter method
   (c) Sample the global factors $\bar{F}_t$ from $p(F_t|y_t, \theta, f_t, \alpha_t, H)$ using the Carter and Kohn (1994) algorithm
   (d) Sample the idiosyncratic components α_t from $p(\alpha^f_{i,t}|y_t, \theta, f_t, \bar{F}_t, H)$ using the Carter and Kohn (1994) algorithm
   (e) Sample the block H from $p(H|y_t, \theta, f_t, \bar{F}_t, \alpha_t)$
      i. Compute y_t^* and run the loop (ii) - (iv) 2000, burning the results of the first 500 iterations
      ii. Sample the states s_t from $p(s_t|y_t^*, h_t, \mu_h, \pi, \sigma_h, \Theta_{\text{-}})$
      iii. Sample each process of h_t from $p(h_t^F|y_t^*, s_t, \mu_h, \pi, \sigma_h, \Theta_{\text{-}})$ using the Carter and Kohn (1994) algorithm
      iv. Sample each pair of μ_h and π from $p(\mu_{h^F}, \pi^F|y_t^*, h_t, s_t, \Theta_{\text{-}}) \sim$ N
      v. Sample each diagonal element of Σ_h from $p(\sigma^2_{h^F}|y_t^*, h_t, s_t, \mu_h, \pi, \Theta_{\text{-}}) \sim$ IG

B Derivation of the Posterior Distributions

B.1 Derivation of the Time-Invariant Parameter Posterior Distributions

In this section, I show the derivations of the time-invariant parameter posterior distributions used in the Gibbs Sampler in section 3.2 and explain how to sample from them. For simplicity, define Θ^- as the subset of all elements minus the sampled parameter.

1. Sample the diagonal elements σ_x^2 (where x denotes a placeholder for v, u, e, or h) of Σ_v, Σ_u, Σ_e, and Σ_h from the Inverse Gamma conditional posterior distribution:

$$\sigma_x^2 \mid y_t, \Theta^- \sim \text{IG}\left(a + \frac{T}{2}, b + \sum_{t=1}^{T} u_t^2\right),$$

   where $\sum_{t=1}^{T} u_t^2$ denotes the sum of squared errors for the corresponding variance element. The shape parameter a and scale parameter b are derived from the prior distribution $\text{IG}(a, b)$, and differ for each covariance matrix. The use of non-informative priors implies $a = 0.001$ and $b = 0.001$ for all covariance elements.

2. Sample the elements β_i^f in B. With a prior $\underline{\beta_i^f} = 0$ and $\underline{V_i^f} = 10^4$, the posterior of β_i^f is sampled from $\beta_i^f | y_t, \Theta^- \sim \text{N}(\bar{\beta}_i^f, \bar{V}_i^f)$, where

$$\bar{V}_i^f = \left[\sum_{t=1}^{T} \frac{F_t^2}{\sigma_{e_i^f}^2} + \frac{1}{\underline{V_i^f}}\right]^{-1}$$

   and

$$\bar{\beta}_i^f = \bar{V}_i^f \left[\sum_{t=1}^{T} \frac{f_{i,t} F_t}{\sigma_{e_i^f}^2} + \frac{\underline{\beta_i^f}}{\underline{V_i^f}}\right].$$

3. Sample (c^F, ϕ^F). With a truncated normal prior $\underline{\phi^F} = 0$ and $\underline{V^{F_\phi}} = 10^4$ for ϕ^F, the posterior conditional is derived as $\phi^F | y_t, \Theta^- \sim \text{TN}(\bar{\phi^F}, \bar{V}^{F_\phi}) \cdot \text{I}[|\phi^F| < 1]$, where

$$\bar{V}^{F_\phi} = \left[\sum_{t=2}^{T} \frac{(F_{t-1})^2}{\omega_t^F} + \frac{1}{\underline{V^{F_\phi}}}\right]$$

and

$$\bar{\phi}^F = \bar{V}^{F_\phi}\left[\sum_{t=2}^{T}\frac{(F_t - c^F)(F_{t-1})}{\omega_t^F} + \frac{\underline{\phi}^F}{\underline{V}^{F_\phi}}\right].$$

For identification, estimate $C = (\mathrm{I} - \Phi)\mu_F$ with the latest draws of Φ and F_t.

4. Sample (γ_i^f, ψ_i^f). With a truncated normal prior $\underline{\psi}^f = 0$ and $\underline{V}^{f_\psi} = 10^4$ for each ψ_i^f, the posterior conditional is derived as $\psi_i^f | y_t, \Theta^- \sim \mathrm{TN}(\bar{\psi}^f, \bar{V}^{f_\psi}) \cdot \mathrm{I}[|\psi_i^f| < 1]$, where

$$\bar{V}^{f_\psi} = \left[\sum_{t=1}^{T}\frac{(\alpha_{i,t-1}^f)^2}{\sigma_{u_i^f}^2} + \frac{1}{\underline{V}^{f_\psi}}\right]$$

and

$$\bar{\psi}_i^f = \bar{V}^{f_\psi}\left[\sum_{t=2}^{T}\frac{(\alpha_{i,t}^f - \gamma_i^f)(\alpha_{i,t-1}^f)}{\sigma_{u_i^f}^2} + \frac{\underline{\psi}^f}{\underline{V}^{f_\psi}}\right].$$

For identification, estimate $\Gamma = (\mathrm{I} - \Psi)\mu_\alpha$ with the latest draws of Ψ and α_t.

5. Sample (μ_{h^F}, π^F). The posterior of μ_{h^F} is derived as $\mu_{h^F} | y_t, \Theta^- \sim \mathrm{N}(\bar{\mu}_{h^F}, \bar{V}^h)$, with a prior $\underline{\mu}_{h^F} = 0$ and $\underline{V}^h = 10^4$, where

$$\bar{V}^h = \left[\sum_{t=1}^{T}\frac{(1-\pi^F)^2}{\sigma_{h^F}^2} + \frac{1}{\bar{V}^h}\right]^{-1}$$

and

$$\bar{\mu}_{h^F} = \bar{V}^h\left[\sum_{t=1}^{T}\frac{(1-\pi^F)(h_t^F - \phi^F h_{t-1}^F)}{\sigma_{h^F}^2} + \frac{\underline{\mu}_{h^F}}{\underline{V}^h}\right].$$

With a truncated normal prior $\underline{\pi}^F = 0$ and $\underline{V}^{F_\pi} = 10^4$ for ϕ^F, the posterior conditional is derived as $\pi^F | y_t, \Theta^- \sim \mathrm{TN}(\bar{\pi}^F, \bar{V}^{F_\pi}) \cdot \mathrm{I}[|\pi^F| < 1]$, where

$$\bar{V}^{F_\pi} = \left[\sum_{t=2}^{T}\frac{(h_{t-1}^F - \mu_{h^F})^2}{\sigma_{h^F}^2} + \frac{1}{\underline{V}^{F_\pi}}\right]$$

and

$$\bar{\pi}^F = \bar{V}^{F_\pi}\left[\sum_{t=2}^{T}\frac{(h_t^F - \mu_{h^F})(h_{t-1}^F - \mu_{h^F})}{\sigma_{h^F}^2} + \frac{\underline{\pi}^F}{\underline{V}^{F_\pi}}\right].$$

B.2 Derivation of the Country Factors Posterior Distribution

Recall the state-space representation for the country factors stored in the vector f_t

$$\begin{aligned} y_t &= \Pi(\lambda) f_t + v_t, & v_t &\sim \mathcal{N}(0, \Sigma_v), \\ f_t &= \alpha_t + \mathrm{B}\bar{F}_t + e_t, & e_t &\sim \mathcal{N}(0, \Sigma_e). \end{aligned}$$

To draw the country factors f_t in Step 2b of the Gibbs sampler, we derive the conditional posterior distribution $p(f_t|y_t, \alpha_t, B, \bar{F}_t)$. Define $x_t = \{\alpha_t, \bar{F}_t\}$, and note that the country factors f_t are not subjected to dynamic properties. Therefore, there is no need for a backwards recursion method and only the noise e_t has to be filtered out of f_t, through the Kalman Filter. In particular, I exploit the normal distribution lemma

$$\begin{pmatrix} y_t \\ f_t \end{pmatrix} \Bigg| \, x_t \sim \mathrm{N}\left(\begin{pmatrix} y_{t|x_t} \\ f_{t|x_t} \end{pmatrix}, \begin{pmatrix} V[y_{t|x_t}] & Cov[y_{t|x}, f_{t|x_t}] \\ Cov[f_{t|x_t}, y_{t|x_t}] & V[f_{t|x_t}] \end{pmatrix} \right),$$

where

$$\begin{aligned} y_{t|x_t} &= \mathbb{E}[y_t|x_t] = \Pi(\lambda)(\alpha_t + \mathrm{B}\bar{F}_t) \\ f_{t|x_t} &= \mathbb{E}[f_t|x_t] = \alpha_t + \mathrm{B}\bar{F}_t \\ V[y_{t|x_t}] &= V[v_t + \Pi(\lambda)e_t] = \Sigma_v + \Pi(\lambda)\Sigma_e\Pi(\lambda)' \\ Cov[y_{t|x_t}, f_{t|x_t}] &= \Pi(\lambda)Cov[f_{t|x_t}, f_{t|x_t}] = \Pi(\lambda)\Sigma_e \\ Cov[f_{t|x_t}, y_{t|x_t}] &= Cov[f_{t|x_t}, f_{t|x_t}]\Pi(\lambda)' = \Sigma_e\Pi(\lambda)' \\ V[f_{t|x_t}] &= \Sigma_e, \end{aligned}$$

to obtain the conditional posterior distribution $f_t|y_t, x_t \sim \mathcal{N}(f_{t|t}, V[f_{t|t}])$. The normal distribution lemma gives

$$\begin{aligned} f_{t|t} &= f_{t|x_t} + Cov[f_{t|x_t}, y_{t|x_t}]V[y_{t|x_t}]^{-1}\left(y_t - y_{t|x_t}\right), \\ V[f_{t|t}] &= V[f_{t|x_t}] - Cov[f_{t|x_t}, y_{t|x_t}]V[y_{t|x_t}]^{-1}Cov[y_{t|x_t}, f_{t|x_t}]. \end{aligned}$$

B.3 Derivation of the Carter and Kohn algorithm

The processes F_t, α_t, and h_t are estimated using the algorithm proposed by Carter and Kohn (1994). This algorithm proposes that a latent time series can be sampled using the Kalman Filter and Smoother. This section explains the algorithm in general form and specifies it for each process. Use the state-space representation

$$y_t = A_t + H\xi_t + v_t \qquad v_t \sim \mathrm{N}(0, R), \tag{26}$$

$$\xi_t = C + F\xi_{t-1} + u_t \qquad u_t \sim \mathrm{N}(0, Q_t), \tag{27}$$

to start the Kalman Filter for $t = 1, ..., T$. The prediction step is summarized by

$$\begin{aligned} \xi_{t|t-1} &= C + H\xi_{t-1} \\ P_{t|t-1} &= HP_{t-1|t-1}H' + Q_{t-1} \end{aligned}$$

and followed by the updating step

$$\begin{aligned} K &= P_{t|t-1}H' \cdot \left[HP_{t|t-1}H' + R\right]^{-1} \\ \xi_{t|t} &= \xi_{t|t-1} \cdot [y_t - (A_t + H\xi_t)] \\ P_{t|t} &= [\mathrm{I} - KH] \cdot P_{t|t-1}. \end{aligned}$$

The filter is followed by a backwards smoothing algorithm, the Kalman Smoother. Given the sample T, the previous results are used to iterate backwards and compute the smoothed estimates, starting at $T - 1$, from recursion

$$\begin{aligned} J_t &= P_{t|t}F'P_{t+1|t}^{-1}, \\ \xi_{t|T} &= \xi_{t|t} + J_t(\xi_{t+1|T} - \xi_{t+1|t}), \\ P_{t|T} &= P_{t|t} + J_t(P_{t+1|T} - P_{t+1|t})J_t'. \end{aligned}$$

The sampling proceeds as follows: at $t = T$ the unobserved states are sampled using $\xi_{T|T} \sim \mathrm{N}(\xi_{T|T}, P_{T|T})$. Then, for $t = T - 1, ..., 1$, we sample the states as $\xi_{t|T} \sim \mathrm{N}(\xi_{t|T}, P_{t|T})$. To specify each process, fit the state space representation shown in section 3.1, in eq. (26) - (27). For more details, consider C.-J. Kim, Nelson, et al. (1999).

C Data and Tickers

Table 10: Yield Tickers by Country and Maturity

Country	Maturity	Ticker
Germany	3M	DE3MT=RR
	6M	DE6MT=RR
	1Y	DE1YT=RR
	2Y	DE2YT=RR
	3Y	DE3YT=RR
	5Y	DE5YT=RR
	7Y	DE7YT=RR
	10Y	DE10YT=RR
United States	3M	US3MT=RR
	6M	US6MT=RR
	1Y	US1YT=RR
	2Y	US2YT=RR
	3Y	US3YT=RR
	5Y	US5YT=RR
	7Y	US7YT=RR
	10Y	US10YT=RR
Japan	3M	JP3MT=RR
	6M	JP6MT=RR
	1Y	JP1YT=RR
	2Y	JP2YT=RR
	3Y	JP3YT=RR
	5Y	JP5YT=RR
	7Y	JP7YT=RR
	10Y	JP10YT=RR
United Kingdom	3M	GP3MT=RR
	6M	GP6MT=RR
	1Y	GP1YT=RR
	2Y	GP2YT=RR
	3Y	GP3YT=RR
	5Y	GP5YT=RR
	7Y	GP7YT=RR
	10Y	GP10YT=RR

Note: This table exhibits the tickers of the government bond yields for all maturities of Germany, the United States, Japan, and the United Kingdom obtained from *Refinitiv Eikon*.

D Estimation Results

Figure 13: Comparison of the Bayesian and OLS Estimates for Country-Specific Level Factors

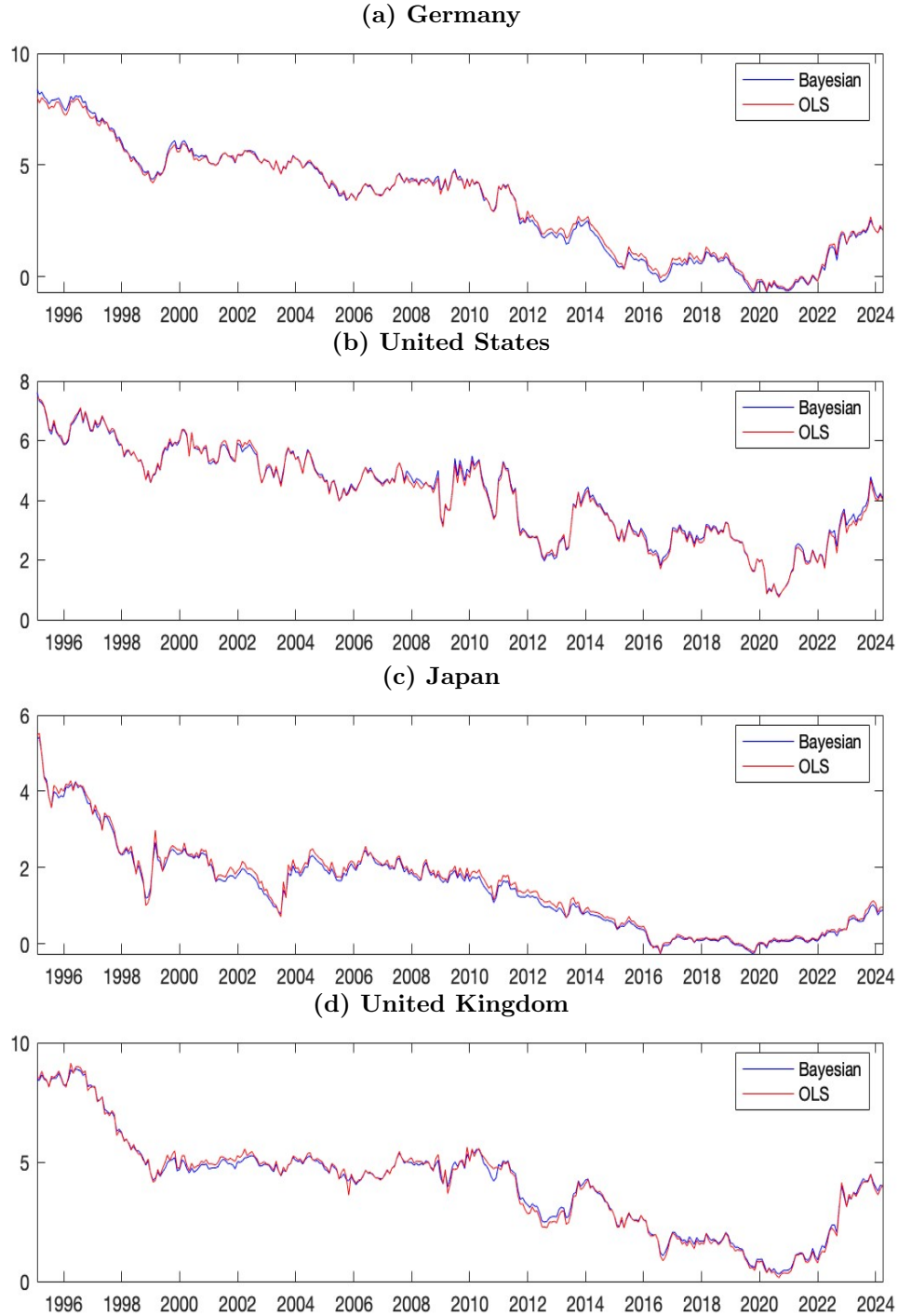

Note: The figure compares the posterior mean of the curvature factors for Germany, the United States, Japan, and the United Kingdom to the level factors obtained through OLS estimation. The analysis covers the sample period from January 1995 to March 2024.

Figure 14: Comparison of the Bayesian and OLS Estimates for Country-Specific Slope Factors

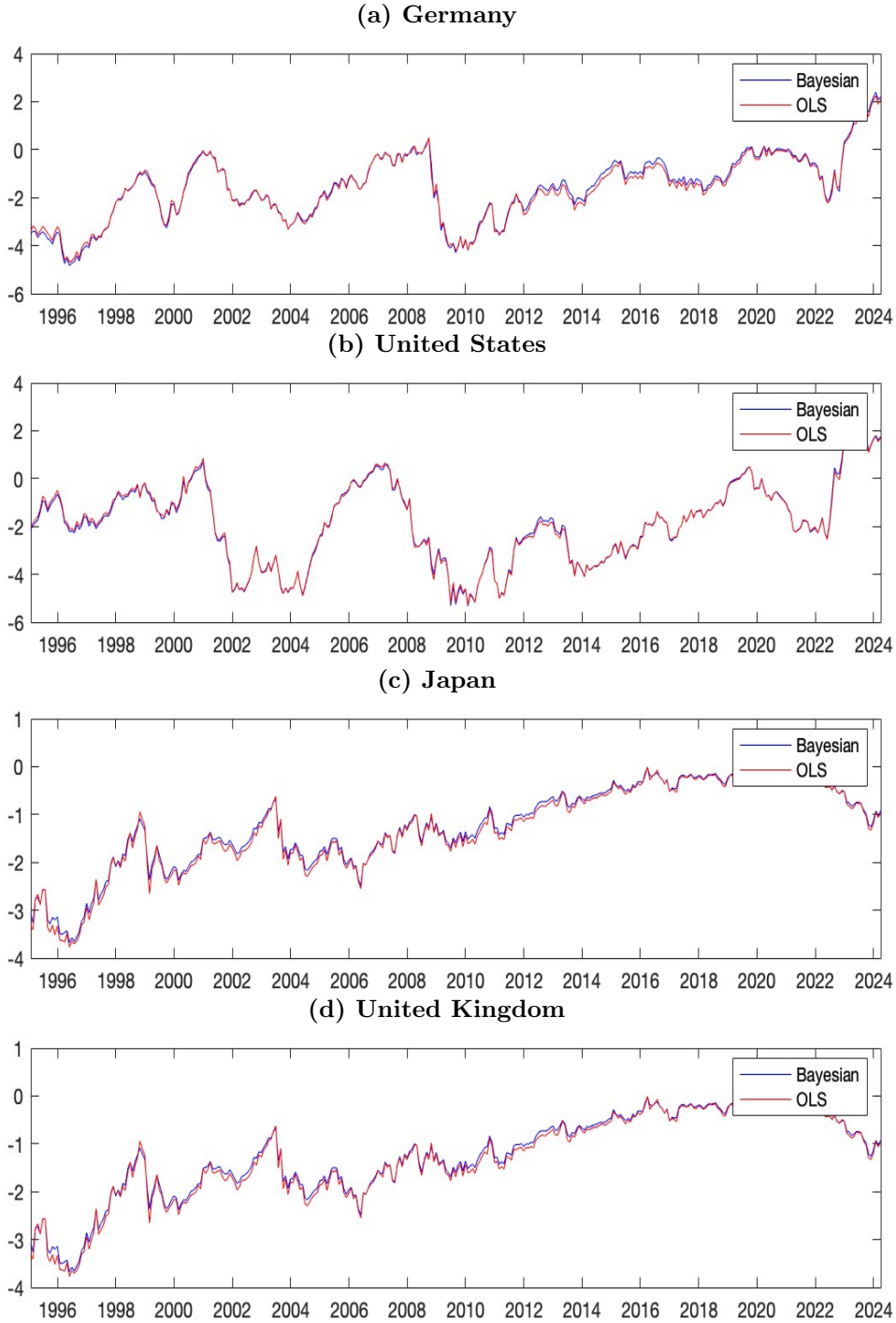

Note: The figure compares the posterior mean of the slope factors for Germany, the United States, Japan, and the United Kingdom to the curvature factors obtained through OLS estimation. The analysis covers the sample period from January 1995 to March 2024.

Figure 15: Comparison of the Bayesian and OLS Estimates for Country-Specific Curvature Factors

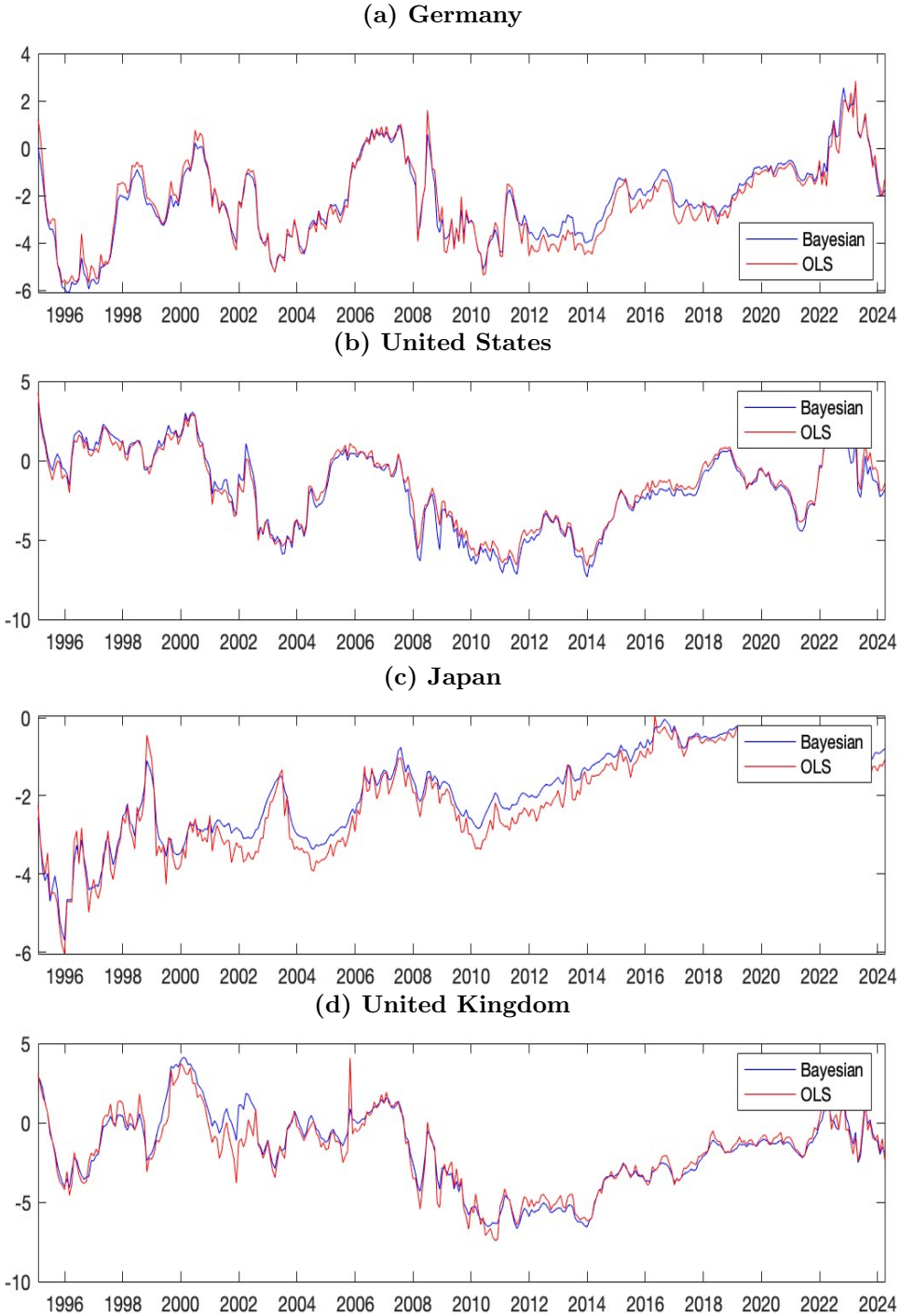

Note: The figure compares the posterior mean of the curvature factors for Germany, the United States, Japan, and the United Kingdom to the curvature factors obtained through OLS estimation. The analysis covers the sample period from January 1995 to March 2024.

Figure 16: The Posterior Mean of the Country-Specific Level Factors with the Posterior Two Standard Deviation Bands

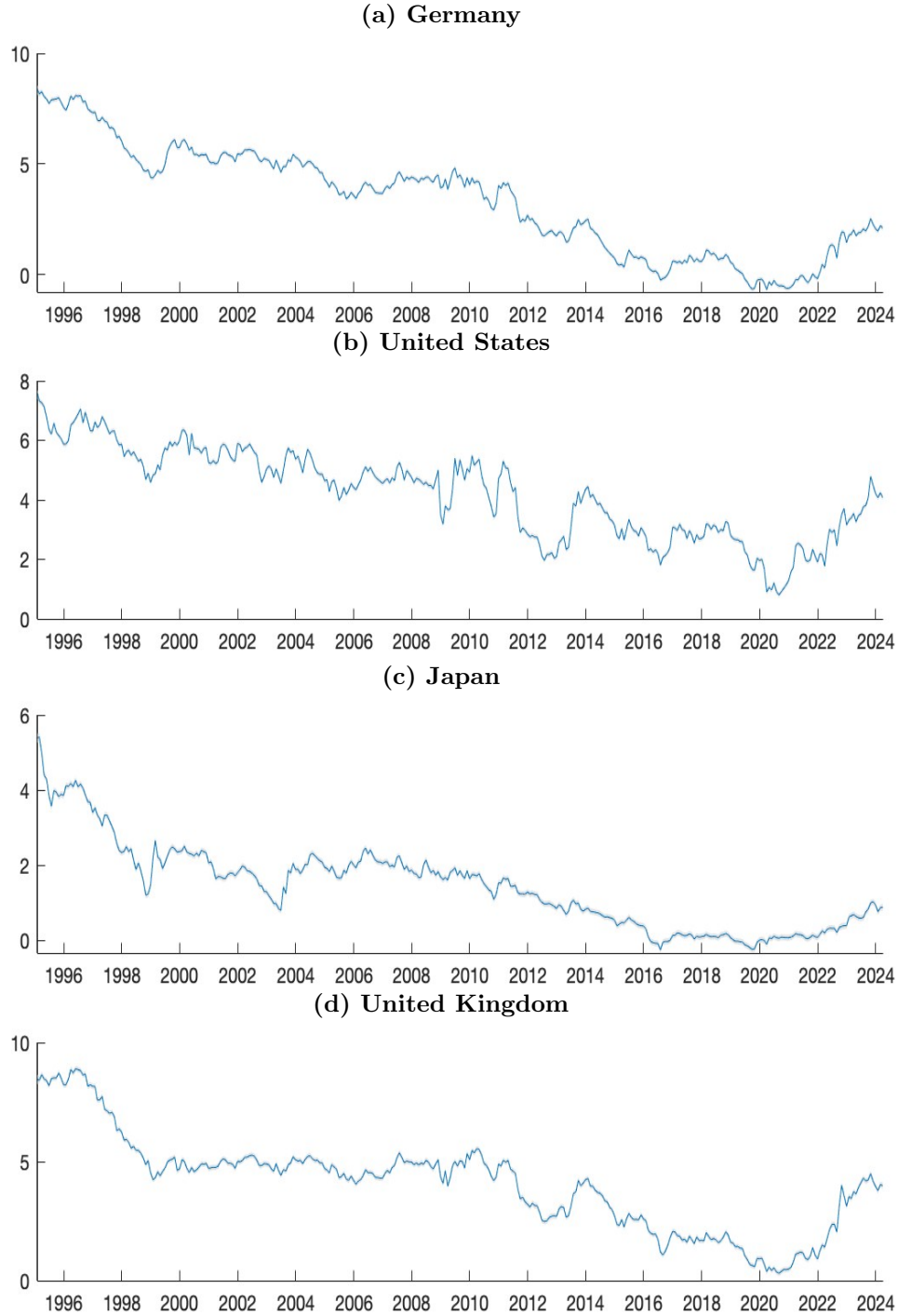

Note: This figure displays the posterior mean of the level factors for Germany, the United States, Japan, and the United Kingdom together with their two posterior standard deviation bands. The analysis covers the sample period from January 1995 to March 2024.

Figure 17: The Posterior Mean of the Country-Specific Slope Factors with the Posterior Two Standard Deviation Bands

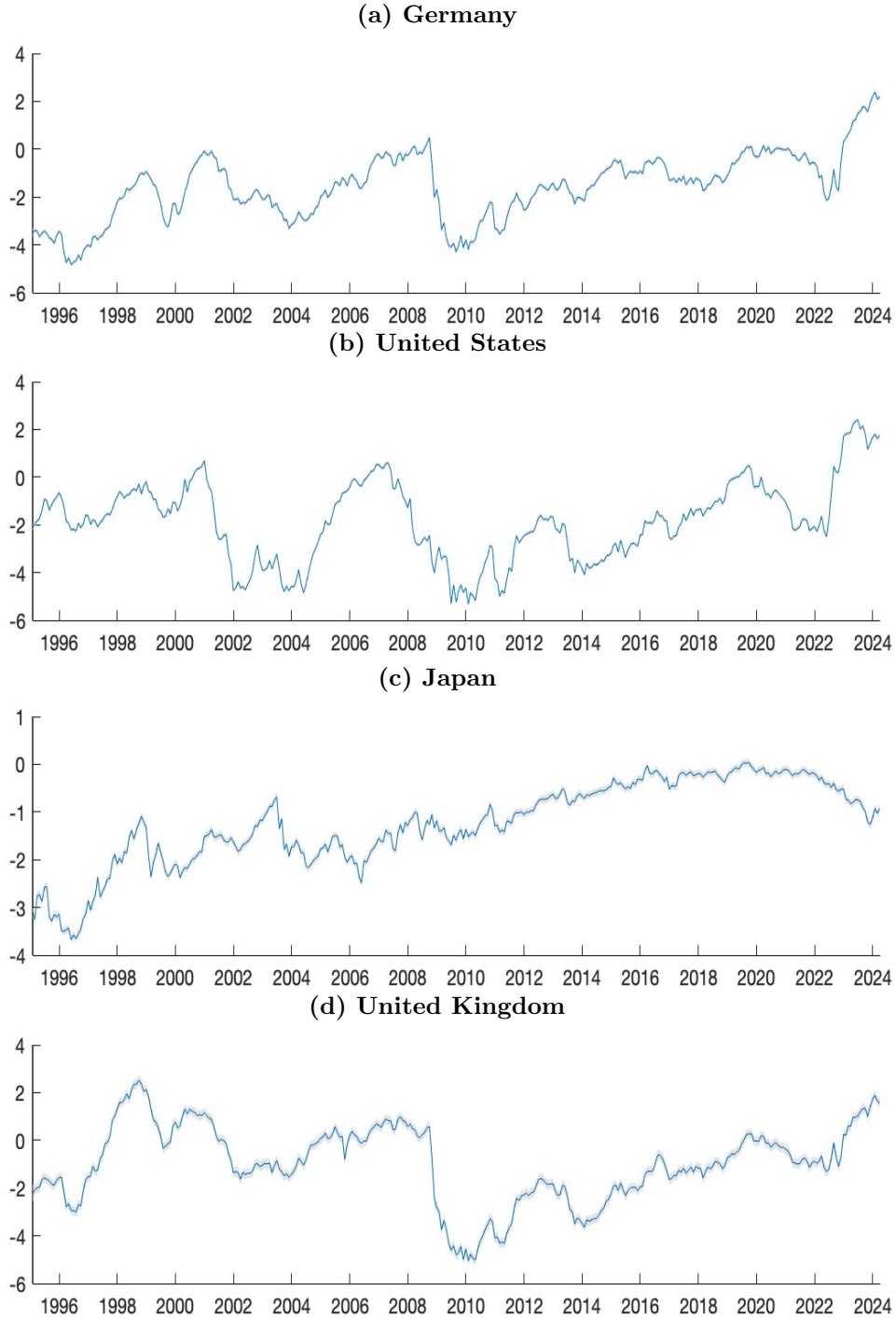

Note: This figure displays the posterior mean of the slope factors for Germany, the United States, Japan, and the United Kingdom together with their two posterior standard deviation bands. The analysis covers the sample period from January 1995 to March 2024.

Figure 18: The Posterior Mean of the Country-Specific Curvature Factors with the Posterior Two Standard Deviation Bands

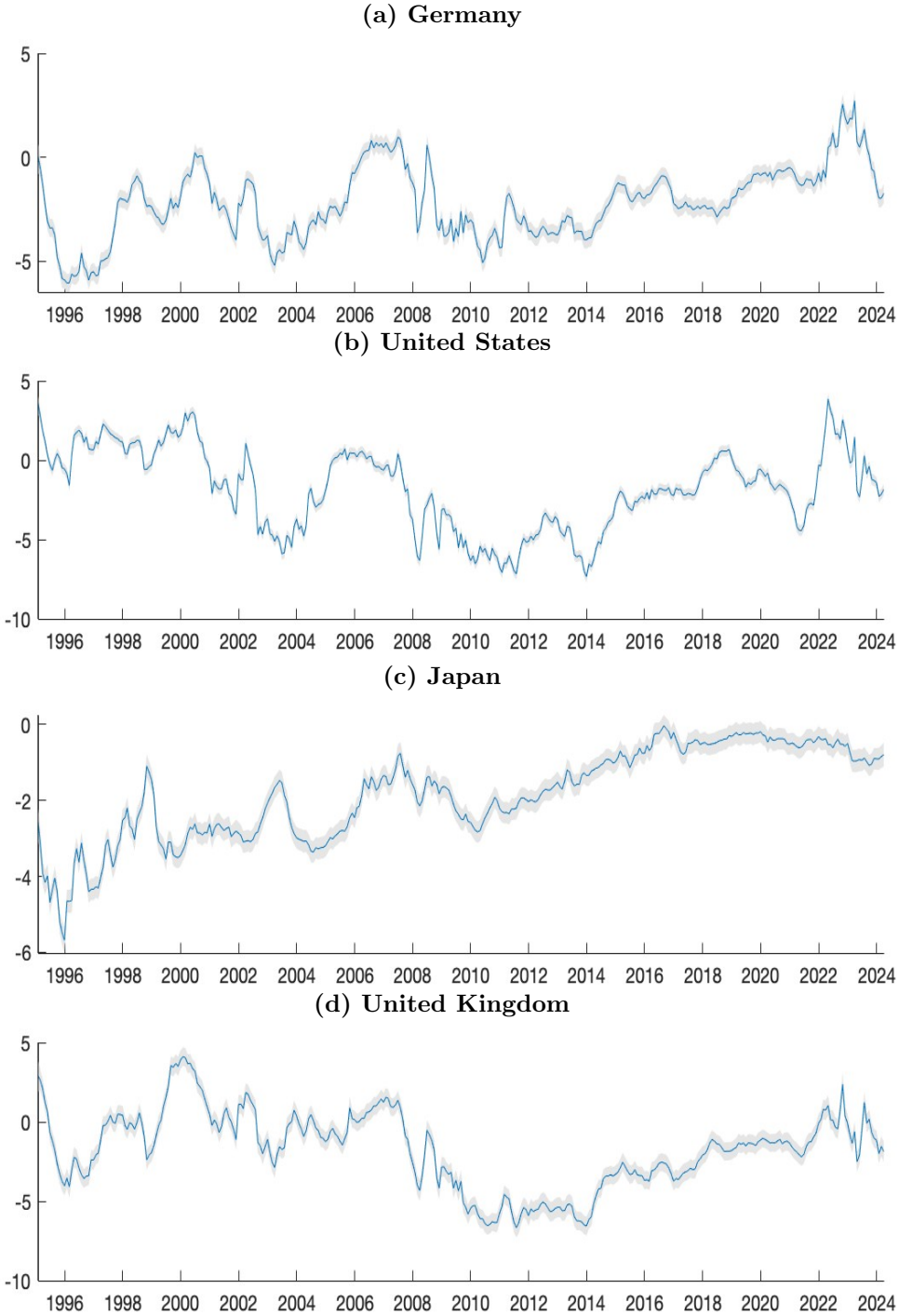

Note: This figure displays the posterior mean of the curvature factors for Germany, the United States, Japan, and the United Kingdom together with their two posterior standard deviation bands. The analysis covers the sample period from January 1995 to March 2024.